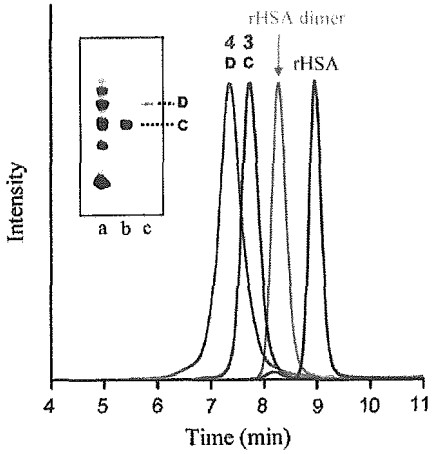

Figure 3. Native-PAGE electrophoresis and HPLC elution curves of the isolated rHSA clusters at 25 °C. In the Native-PAGE pattern, lane a, reaction mixture before purification; lane b, isolated band C; lane c, isolated band D. In the HPLC profiles, red line, rHSA monomer; orange line, rHSA dimer bridged through Cys-34 by BMH; blue line, isolated band C, which corresponds to the rHSA trimer; green line, isolated band D, which corresponds to the rHSA tetramer.

Table 1. Molecular Masses and *pI* Values of rHSA Monomer, Dimer, and Clusters

	M_w		
	obs.[a]	calcd.	p*I*
rHSA[b]	66331	66451	4.8
rHSA dimer[b,c]	132 741	133 180	4.8
band C (rHSA trimer)	200 469	201 614	4.8
band D (rHSA tetramer)	266 538	267 953	4.8

[a] Measured by MALDI-TOF–MS. [b] From ref 7b. [c] rHSA dimer bridged Cys-34 by BMH.

comparison with the protein ladder (lane a), the molecular weights of the bands B, C, and D were estimated to be ca. 130, 200, and 260 kDa, respectively. It can be postulated that they are the rHSA dimer, trimer, and tetramer. The pyridylditio terminates of the core albumin reacted with the single active Cys-34 of the shell albumin creating albumin clusters. The HPLC profile of the reaction mixture exhibited broad multiple bands in the range of 6.5–8.5 min before the rHSA peak (9.0 min; Figure 2). From the careful inspection of the elution curve by peak fitting simulation, we could divide the entire pattern into six components (peaks 1–6). Most probably, the peaks 2–6 correspond to the rHSA dimer to hexamer. Gel permeation chromatography also showed a similar elution curve. Several synthesis repetitions always gave the same patterns in Native-PAGE, HPLC, and GPC. The fractions whose Native-PAGE showed bands C and D were then corrected (Figure 3, inset lanes b and c). Their HPLC profiles exhibited a sharp peak at the exactly the same position where we predicted for peaks 3 and 4 in Figure 2.

The MALDI-TOF–MS of the components of peaks 3 (band C) and 4 (band D) showed a molecular masses at *m/z* 200 469 and 266 538, respectively, which are in good agreement with the calculated value of the rHSA trimer and tetramer (M_w = 201 614 and 267 953) within a difference of 0.5% (Table 1). We first isolated the well-defined rHSA trimer and tetramer in which the Lys groups of the core

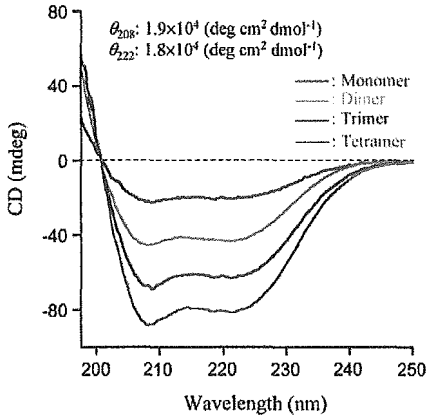

Figure 4. CD spectra of rHSA monomer, dimer bridged through Cys-34 by BMH and clusters in PBS solution (pH 7.4) at 25 °C.

albumin are covalently bridged by the Cys-34 group of the shell albumins.

The peak area evaluations for the six components in Figure 2 indicated their molar ratios in the reaction mixture; monomer (88.2%), dimer (3.1%), trimer (4.3%), tetramer (2.5%), pentamer (1.4%), and hexamer (0.5%). Because the average degree of polymerization was 3.3, we estimated the reaction ratio (X) of the PDPH–rHSA

$$\text{reacted PDPH–rHSA:unreacted (PDPH–rHSA + SH–rHSA)} = X:(1 - X) + (10 - 2.3X) = 11.8:88.2 \quad (3)$$

Thus, X was calculated to be 1.0; this means that all of the PDPH–rHSA (core albumin) participated in the reaction with the shell albumin. The formation ratio of each cluster can be estimated; dimer (26%), trimer (36%), tetramer (22%), pentamer (12%), and hexamer (4%).

The CD spectral patterns (λ_{min} = 208 and 222 nm) and the molar ellipticities at 208 and 222 nm ($[\theta]_{208} = 1.9 \times 10^4$ deg cm^2 dmol^{-1}, $[\theta]_{222} = 1.8 \times 10^4$ deg cm^2 dmol^{-1}) of the isolated rHSA trimer and tetramer were identical to those of the monomer and dimer (Figure 4).[4b,7b] Their isoelectric points (pI = 4.8) were also identical to that of rHSA (Table 1). These results implied that the secondary/tertiary structure, the α-helix content, and surface net charges of the rHSA units were intact after the cluster formation.

TEM of the negatively stained samples of the rHSA tetramer showed homogeneous particles with a diameter of 20–30 nm (Figure 5a,b). The appearance of the cluster solutions was unchanged for over one year and underwent no aggregation and precipitation. We postulate that one tetramer consists of four rHSA molecules bound in the trigonal pyramid form, which was drawn as a model in Figure 5c. rHSA involves a total of 59 Lys groups, and the cross-linker SPDPH can statistically bind to the surface. On the basis of the assay of the dithiopyridyl group, we found that the 8.3 functional PDPH arms are introduced into the core albumin. The shell albumins (SH–rHSAs) therefore approach the PDPH–rHSA from all directions to form a disulfide bridge with Cys-34. As a consequence, the conformation of the tetramer should become a trigonal pyramid-like structure, which is the most favorable arrangement to avoid the steric repulsion of the albumin units.

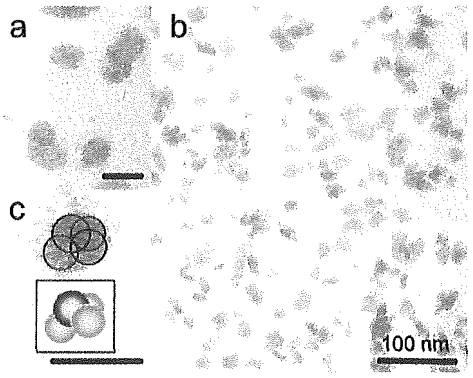

Figure 5. TEM observations of negatively stained rHSA tetramer. In panels a and c, the scale bars indicate the length of 30 nm. In panel c, the trigonal pyramid form of the rHSA tetramer is predicted from the one molecule under magnification.

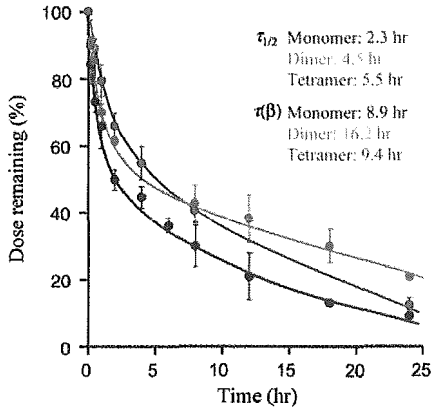

Figure 6. Plasma levels of ^{125}I–rHSA tetramer after intravenously administration to Wistar rats (rHSA amount = 1.0 mg kg^{-1}). The data for the ^{125}I–rHSA monomer and dimer were cited from our previously reported paper (ref 7b). All values are mean ± S. D. (n = 3).

Circulation Lifetime of ^{125}I-Labeled rHSA Tetramer in Rats. The rHSA tetramer labeled with ^{125}I was injected into anesthetized rats to determine the blood circulation lifetimes. Throughout the experiments, the turbidity of the plasma phase and the blood cell numbers were constant, showing no aggregation of the albumin clusters and blood cell components. The time courses of the radioactivity demonstrated two-phase kinetics and significant differences from the monomer's decay (Figure 6). The half-lifetime ($\tau_{1/2}$, time when the initial value decreased to 50%) of the rHSA tetramer was 5.5 h, which was 2.4-fold longer than that of the monomer (2.3 h).[7b] This was due to the low ratio of the distribution phase (α-phase) of the tetramer (26%), compared to the monomer and dimer, 39% and 36%, respectively. The increase in the molecular size led to retardation of the extravasation through the vascular endothelium. On the contrary, its lifetime (τ) of the disappearance phase (β-phase; 8.9 h) was shorter than the tightly bridged rHSA dimer with a sulfide bond (16.2 h); although the $\tau_{1/2}$ of the dimer is lower than the tetramer, there is a greater amount of dimer at 24 h than tetramer. The rHSA tetramer disappeared slowly after 12 h, and 10% remained at 24 h from the injection, which was almost the same amount observed in the monomer group. After 12 h, the weak disulfide bonds between the core and shell albumins may be cleaved to dissociate the monomer components and cleared from the bloodstream. Radioactivity of the trichloroacetic acid precipitates recovered up to 90% of the intensity, which means ^{125}I did not dissociate from the proteins. The tissue distributions of the rHSA tetramer were in the skin, liver, and spleen, and there were no differences to that of the rHSA monomer. Our albumin tetramer may become a unique vehicle which serves to sustain a high drug concentration particularly during the initial phase.

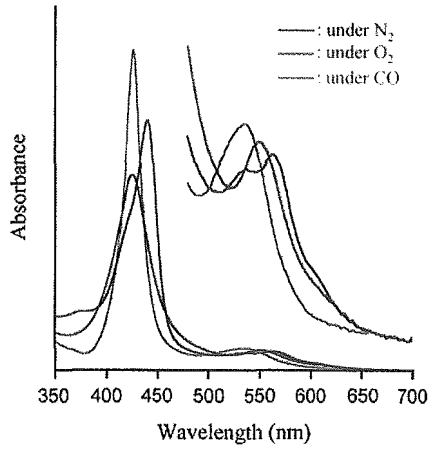

Figure 7. UV–vis absorption spectral changes of the rHSA–FeP tetramer in phosphate-buffered solution (pH 7.3) at various conditions (25 °C).

Albumin–Heme Clusters and Their O_2 Binding. Mixing the ethanolic FeP with an aqueous albumin cluster and removing the ethanol by ultrafiltration produced red-colored homogeneous albumin–heme cluster solutions. They were rather stable and stored for more than 1 year at 4 °C without any precipitation. From the quantitative assays of rHSA and FeP, the molar ratios of the FeP/rHSA were determined to be 24.2 and 31.6 for the trimer and tetramer, which are 3- and 4-fold molar excess amounts of the monomeric rHSA–FeP. We can conclude that a maximum of eight FePs were also incorporated into the rHSA unit. These albumin–heme clusters showed identical CD spectra and pI values (4.8) with the original rHSA trimer and tetramer, which implied that the FeP incorporation did not cause any structural changes in the albumin components.

The UV–vis absorption spectrum of the aqueous rHSA–FeP tetramer in an N_2 atmosphere showed the formation of a five-coordinate high-spin complex involving an axially bound 2-methylimidazolyl side-chain (λ_{max} = 444, 539, and 565 nm; Figure 7).[4b,8,13] After this solution was kept under a stream of O_2 for 5 min, the absorption spectra changed to that of a typical O_2–adduct complex (λ_{max} = 426 and 549 nm).[4b,8,13] This dioxygenation was reversibly observed and dependent on the O_2/N_2 pressure under physiological conditions (pH 7.3, 37 °C). After admitting the CO gas, the O_2–adduct complex immediately moved to the carbonyl low-spin complex (λ_{max} = 427 and 539 nm). The rHSA-FeP trimer also showed identical spectral changes under these conditions [rHSA-FeP trimer in N_2 (λ_{max} = 442, 539, and 564 nm), O_2 (λ_{max} = 423 and 547 nm), and CO atmosphere (λ_{max} = 426 and 534 nm)].

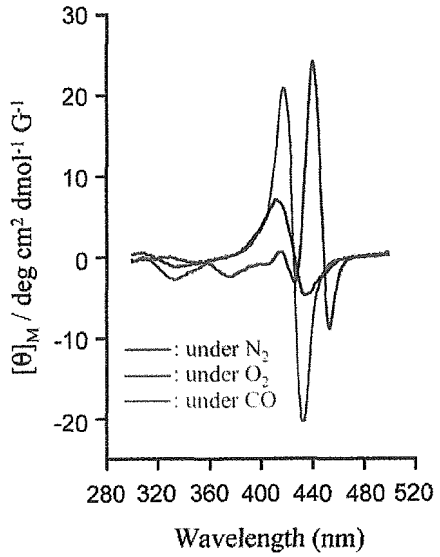

Figure 8. MCD spectral changes of the rHSA–FeP tetramer in phosphate-buffered solution (pH 7.3) at various conditions (25 °C).

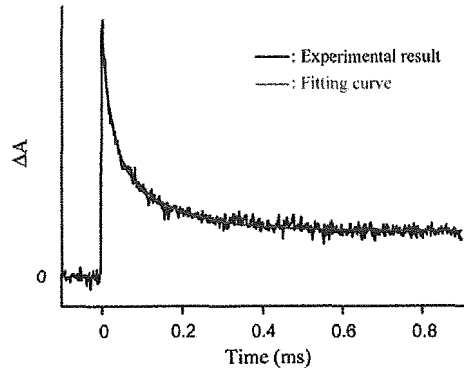

Figure 9. Absorption decay of O_2 rebinding to the rHSA–FeP cluster in phosphate-buffered solution (pH 7.3) after the laser flash photolysis at 25 °C. The kinetics was composed of three phases and relaxation curve was fitted by triple-exponentials.

MCD spectroscopy revealed the coordination structure of the FeP in the rHSA clusters. Under an N_2 atmosphere, the MCD of the rHSA-FeP tetramer resembled the well-characterized spectrum of a mono-imidazole ligated five-*N*-coordinate high-spin tetraphenylporphinatoiron(II) (Figure 8).[14] This observation indicates that the amino acid residue in the rHSA structure did not bind to the sixth position of FeP. The admission of O_2 gas changed the spectrum to an S-shaped A-term MCD in the Soret-band region, which shows the formation of an O_2–adduct complex.[14] The CO adduct is also low spin and exhibited a similar A-term MCD band with a high intensity.

The autoxidation reaction of the oxy state (λ_{max} = 549 nm) slowly occurred and the absorption intensity of 549 nm almost disappeared after 48 h, leading to the formation of the inactive Fe(III)P. The half-lives of the dioxygenated species ($\tau_{1/2}$) of the rHSA–FeP trimer and tetramer were both 7 h at 37 °C, which are almost the same as that of our previous results for the rHSA–FeP dimer ($\tau_{1/2}$ = 6 h).[7b]

O_2-Binding Kinetics and Equilibrium of Albumin–Heme Clusters. Flash photolysis experiments for the albumin–heme clusters were performed to determine the association and dissociation rate constants of O_2 (k_{on}, k_{off}). We have shown that the O_2 associations to FePs in the monomeric rHSA are affected by the molecular environments around the FeP site, for example, steric hindrance of the nearest amino acid residues.[4c] In the case of the albumin–heme clusters, there should be multiple kinetic parameters. Nevertheless, the O_2 binding profile to FeP demonstrated the same trends as the rHSA–FeP monomer. The absorption change accompanying the O_2 recombination clearly obeyed three-phases, which were fit by a triple-exponential kinetics (Figure 9). The fastest minor component (k_1) is related to a base dissociation reaction.[15] The linear relationship between the apparent rates k_2 and k_3 vs the [O_2] provided two association rate constants for the fast O_2 rebinding (k_{on}) and the slow O_2 rebinding (k'_{on}; Table 2). The k_{on} values are 4.1–7.8-fold greater than k'_{on}, and the amplitude ratios of the fast and slow phases were approximately 1/1, which implied that half of the FeP molecules in the rHSA trimer and tetramer may locate in the slow sites for the O_2 association. The O_2-binding affinity ($P_{1/2}$) of the rHSA-FeP clusters were determined to be 38 Torr at 37 °C on the basis of the UV–vis. absorption spectral changes by O_2 titration with different [O_2].[4b,8,13] The obtained $P_{1/2}$ is close to that of the rHSA–FeP monomer and human RBC (Table 2).[8,16,17] The cluster formation did not alter the O_2-binding properties of rHSA–FeP.

Table 2. O_2-Binding Parameters of rHSA-FeP Monomer, Dimer, and Clusters in Phosphate-Buffered Solution (pH 7.3) at 25 °C

	10^{-6} k_{on} (M^{-1} s^{-1})	10^{-6} K_{on} (M^{-1} s^{-1})	10^{-2} k_{off} (s^{-1})	10^{-2} K_{off} (s^{-1})	$P_{1/2}$ (Torr)[a]
rHSA-FeP[b]	46	7.3	9.8	1.6	13 (35)
rHSA-FeP dimer[c]	28	4.8	6.7	1.2	15 (38)
rHSA-FeP trimer	46	5.9	8.7	1.1	12 (38)
rHSA-FeP tetramer	53	13	11	2.7	12 (38)
Hb(T-state)α[d]	2.9		1.8		40
human RBC[e]					8 (27)

[a] At 37 °C in parenthesis. [b] From ref 8. [c] From ref 7b. [d] Hbα chain (monomer), aqueous pH 7.0–7.4, 20 °C, from ref 16. [e] From ref 17.

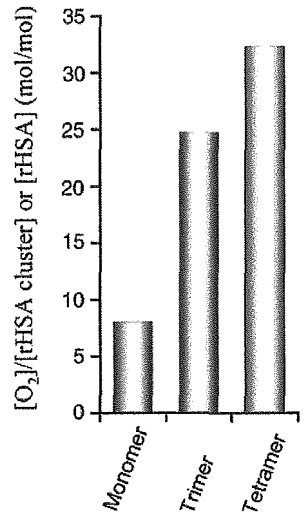

Figure 10. Molar ratio of the increased O_2 per rHSA cluster (mol/mol) after exposure of CO gas to rHSA–FeP cluster solutions (25 °C).

O_2 Concentration in Albumin−Heme Cluster Solution. The addition of small amounts of CO to the aqueous solutions of the dioxygenated rHSA−FeP clusters ([FeP] = 50 μM) in closed tubes dissociates the coordinated O_2, which immediately diffuses in the medium. In all cases, the O_2 concentrations increased 0.05 mM after the CO exposure. The UV−vis absorption spectra of the solutions changed to that of the carbonyl complex. The molar ratio of the chemically bound O_2 per albumin vehicle ([rHSA cluster] or [rHSA]) (mol/mol) showed that the albumin−heme clusters bind a large volume of O_2 relative to the monomer (Figure 10). The rHSA-FeP tetramer solution ([rHSA tetramer] = 0.75 mM, [heme] = 24 mM) could probably transport a 2.6-fold greater volume of O_2 compared to human blood ([heme] = 9.2 mM) while maintaining the colloid osmotic pressure on a physiological level.

Conclusions

The structurally defined albumin clusters prepared using a unique SH group of Cys-34 reported here provide the following characteristics.

(i) Essential properties of the rHSA units (the secondary/tertiary structure, surface net charges) were intact after the cluster formation. Our albumin clusters behave as a gigantic serum albumin.

(ii) The tetramer showed a longer half-life (5.5 h) in the bloodstream of rats compared to that of the monomer due to the low ratio of the α-phase (26%). However, it slowly disappeared after 12 h and was 10% of the basal value at 24 h after the injection.

(iii) The rHSA unit in the clusters can incorporate a maximum of eight FeP molecules, that is, the trimer and tetramer contain 24 and 32 active O_2-binding heme sites, which are 6- and 8-fold greater than that of the native tetrameric Hb, respectively. The obtained albumin−heme clusters become huge artificial hemoproteins with molecular weights of 235 and 313 kDa and can reversibly bind O_2 under physiological conditions.

(iv) The albumin−heme tetramer has the capability to transport a 4-fold larger volume of O_2 compared to the corresponding monomer when the albumin vehicle molar concentrations were identical. It implies that the albumin−heme clusters potentially become novel RBC substitutes having a 2.6-fold higher O_2 transporting ability than human blood.

This method of creating albumin clusters should lead to generating defined protein polymers and a new series of functional biomaterials. The preparations of the starburst rHSA dendrimer and linear string of rHSA pearls are now in progress.

Acknowledgment. This work was partially supported by a Grant-in-Aid for Scientific Research (No. 16350093) from JSPS, and a Grant-in-Aid for Exploratory Research (No. 16655049) from MEXT Japan, and a Health Science Research Grant (Regulatory Science, B5-551) from MHLW Japan. Prof. Dr. Koichi Kobayashi (Keio University) and Mr. Hisashi Yamamoto (NIPRO Corp.) are greatly acknowledged for the animal experiments.

References and Notes

(1) Peters, T., Jr. *All about albumin, biochemistry, genetics, and medical applications*; Academic Press: San Diego, CA, 1997; and reference therein.
(2) (a) Kragh-Hansen, U. *Pharmacol. Rev.* **1981**, *33*, 17−53. (b) Kragh-Hansen, U. *Danish Med. Bull.* **1990**, *37*, 57−84.
(3) Sheffield, W. P. *Curr. Drug Targets Cardiovasc. Haematol. Disord.* **2001**, *1*, 1−22.
(4) (a) Komatsu, T.; Hamamatsu, K.; Wu, J.; Tsuchida, E. *Bioconjugate Chem.* **1999**, *10*, 82−86. (b) Tsuchida, E.; Komatsu, T.; Matsukawa, Y.; Hamamatsu, K.; Wu, J. *Bioconjugate Chem.* **1999**, *10*, 797−802. (c) Komatsu, T.; Matsukawa, Y.; Tsuchida, E. *Bioconjugate Chem.* **2000**, *11*, 772−776.
(5) Tsuchida, E.; Komatsu, T.; Matsukawa, Y.; Nakagawa, A.; Sakai, H.; Kobayashi, K.; Suematsu, M. *J. Biomed. Mater. Res.* **2003**, *64A*, 257−261.
(6) Carter, D. C.; Ho, J. X. *Adv. Protein Chem.* **1994**, *45*, 153−203.
(7) (a) Komatsu, T.; Hamamatsu, K.; Tsuchida, E. *Macromolecules* **1999**, *32*, 8388−8391. (b) Komatsu, T.; Oguro, Y.; Teramura, Y.; Takeoka, S.; Okai, J.; Anraku, M.; Otagiri, M.; Tsuchida, E. *Biochim. Biophys. Acta* **2004**, *1675*, 21−31.
(8) Komatsu, T.; Matsukawa, Y.; Tsuchida, E. *Bioconjugate Chem.* **2002**, *13*, 397−402.
(9) Doumas, B. T.; Watson, W. A.; Biggs, H. G. *Clin. Chim. Acta* **1971**, *31*, 87−96.
(10) Grassetti, D. R.; Murray, J. F., Jr. *Arch. Biochem. Biophys.* **1967**, *119*, 41−49.
(11) Pedersen, A. O.; Jacobsen, J. *Eur. J. Biochem.* **1980**, *106*, 291−295.
(12) Watanabe, H.; Yamasaki, K.; Kragh-Hansen, U.; Tanase, S.; Harada, K.; Suenaga, A.; Otagiri, M. *Pharm. Res.* **2001**, *18*, 1775−1781.
(13) Collman, J. P.; Brauman, J. I.; Iverson, B. L.; Sessler, J. L.; Morris, R. M.; Gibson, Q. H. *J. Am. Chem. Soc.* **1983**, *105*, 3052−3064.
(14) (a) Collman, J. P.; Brauman, J. I.; Doxsee, K. M.; Halbert, T. R.; Bunnenberg, E.; Linder, R. E.; LaMar, G. N.; Guadio, J. D.; Lang, G.; Spartalian, K. *J. Am. Chem. Soc.* **1980**, *102*, 4182−4192. (b) Collman, J. P.; Basolo, F.; Bunnenberg, E.; Collins, T. C.; Dawson, J. H.; Ellis, P. E., Jr.; Marrocco, M. L.; Moscowitz, A.; Sessler, J. L.; Szymanski, T. *J. Am. Chem. Soc.* **1981**, *103*, 5636−5648.
(15) Geibel, J.; Cannon, J.; Campbell, D.; Traylor, T. G. *J. Am. Chem. Soc.* **1978**, *100*, 3575−3585.
(16) Sawicki, C. A.; Gibson, Q. H. *J. Biol. Chem. Soc.* **1977**, *252*, 7538−7547.
(17) Severinghous, J. W. *J. Appl. Physiol.* **1966**, *21*, 1108−1116.

BM050454U

Human Serum Albumin Hybrid Incorporating Tailed Porphyrinatoiron(II) in the α,α,α,β-Conformer as an O_2-Binding Site

Akito Nakagawa, Teruyuki Komatsu,* Makoto Iizuka, and Eishun Tsuchida*

Advanced Research Institute for Science and Engineering, Waseda University, 3-4-1 Okubo, Shinjuku-ku, Tokyo 169-8555 Japan. Received June 1, 2005; Revised Manuscript Received October 30, 2005

We have found that recombinant human serum albumin (HSA) incorporating tailed porphyrinatoiron(II) in the α,α,α,β-conformer can reversibly bind and release O_2 under physiological conditions (pH 7.3, 37 °C) like hemoglobin and myoglobin. β-2-Methylimidazolyl-tailed porphyrinatoirons (**6a**, **6b**) are synthesized via four steps from the atropisomers of tetrakis(*o*-aminophenyl)porphyrin. The stereochemistry of the α,α,α,β-conformer has been determined by NMR spectroscopy. **6a** and **6b** form stable O_2-adduct complexes in toluene solution at room temperature. The association rate constants of O_2 are 3.1- and 1.9-fold lower than those of the corresponding α,α,α,α-conformers (**1a**, **1b**), indicating that the three substituents (cyclohexanamide or pivalamide groups) are close to each other on the porphyrin platform and construct a narrow encumbrance around the O_2-coordination site. Although **6a** and **6b** are incorporated into the hydrophobic domains of HSA to produce the albumin–heme hybrid, only HSA-**6a** can bind O_2 in aqueous medium. The cyclohexanamide fences are necessary for the tailed porphyrinatoiron to form a stable O_2-adduct complex under physiological conditions. The O_2-binding affinity ($P_{1/2}$) of HSA-**6a** is 45 Torr (37 °C), and the O_2 transporting efficiency between lungs and muscle tissues in the human body is estimated to be identical to that of human red blood cells. The HSA-**6a** solution will become one of the most promising materials for red blood cell substitutes, which can be manufactured on an industrial scale.

INTRODUCTION

To reproduce the O_2-binding ability of hemoglobin (Hb) and myoglobin (Mb), numerous numbers of model hemes have been synthesized over the past decades (*1*). These continuous approaches, aimed at understanding the precise mechanism of the O_2-binding reaction, have been mostly accomplished in organic solvents, and tetrakis(phenyl)porphyrin (TPP) was widely used as a molecular scaffold. We have also synthesized tetrakis-{α,α,α,α-*o*-(1-methylcyclohexanamido)phenyl}porphinatoiron-(II) bearing a covalently linked proximal imidazole (**1a**, Figure 1)[1] that forms a stable O_2-adduct complex in toluene solution at ambient temperature (*2*). The four cyclohexanamide fences on the distal-side (α-side) of the porphyrin plane are bulky enough to prevent μ-oxo dimer formation, and the 2-methylimidazolyl arm intramolecularly coordinated to the Fe^{2+} center from the proximal-side (β-side) modulates the O_2-binding affinity.

Some substantial efforts have been directed to prepare an artificial O_2 carrier involving a synthetic heme under physiological conditions (pH 7.3, 37 °C), which may become a red blood cell substitute (*1a*, *3*). We have successfully incorporated **1a** into the hydrophobic domains of recombinant human serum albumin (HSA) and found that the albumin–heme hybrid (HSA–**1a**) could reversibly absorb O_2 in aqueous medium (*1a*, *2*, *4*). This red-colored albumin solution showed a long shelf life of over two years without precipitation. More recently,

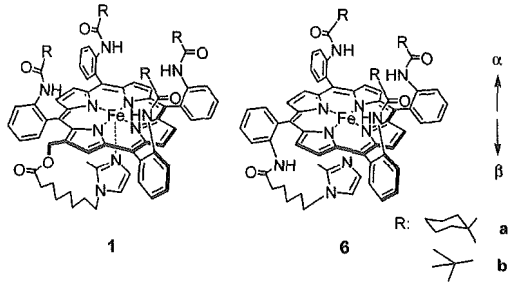

Figure 1. Structures of porphyrinatoiron derivatives in the α,α,α,α-conformer and α,α,α,β-conformer (tailed porphyrinatoiron).

exchange transfusion experiments with HSA–**1a** into anesthetized rats demonstrated that it effectively rescitates the hemorrhagic shock state and transports O_2 to the muscle tissues (*5*). We are now developing this albumin–heme hybrid as an entirely synthetic red blood cell substitute that can be extensively used in a variety of medical situations (*6*).

The only disadvantage of this synthetic heme **1a** is that a great deal of labor is required to make the α,α,α,α (α^4)-conformer and to introduce the imidazolylalkyl arm at the porphyrin periphery via the Vilsmeier reaction (*2*). The starting material, tetrakis(α,α,α,α-*o*-aminophenyl)porphyrin (TAPP), is in a statistical mixture of the four possible atrop isomers (α,α,α,α, α,α,α,β, α,β,α,β, α,α,β,β; the ratio is 1:4:2:1), and the variable α^4-conformer used to be isolated by Lindsey's procedure with a silica gel column separation (*7*). The number of total steps for the synthesis of **1a** is, therefore, eight from TAPP.

In this study, we first incorporated a "tailed porphyrinatoiron" with the $\alpha^3\beta$-conformer as an O_2-binding site of the albumin–heme. A series of tailed porphyrins as the model compound of Hb and Mb were synthesized by Collman and co-worker (*8*). There are two advantages of the tailed porphyrin: (i) the statistical content of the $\alpha^3\beta$-conformer of TAPP is maximum

* Corresponding authors: (E.T.) Tel: +81-3-5286-3120. Fax: +81-3-3205-4740. E-mail: eishun@waseda.jp. (T.K.) E-mail: teruyuki@waseda.jp.

[1] Abbreviations: **1a**: 2-[8-{*N*-(2-methyl-1-imidazolyl)octanoyloxy]-methyl]-5,10,15,20-tetrakis{(α,α,α,α-o-(1-methylcyclohexanamido)-phenyl}porphinatoiron; **1b**: 2-[8-{*N*-(2-methyl-1-imidazolyl)octanoyl oxymethyl]-5,10,15,20-tetrakis{α,α,α,α-*o*-(pivalamido)phenyl}porphinatoiron; **6a**: 5,10,15-Tris {α,α,α-*o*-(1-methylcyclohexanamido)-phenyl}-20-mono[β-*o*-[6-{*N*-(2-methyl-1-imidazolyl)}hexanamido]phenyl]-porphinatoiron; **6b**: 5,10,15-Tris(α,α,α-*o*-(pivalamido)phenyl)-20-mono[β-*o*-[6-{*N*-(2-methyl-1-imidazolyl)}hexyramido]phenyl]-porphinatoiron.

10.1021/bc050154+ CCC: $33.50
Published on Web 12/21/2005

Scheme 1. Synthesis of Tailed Porphyrinatoirons

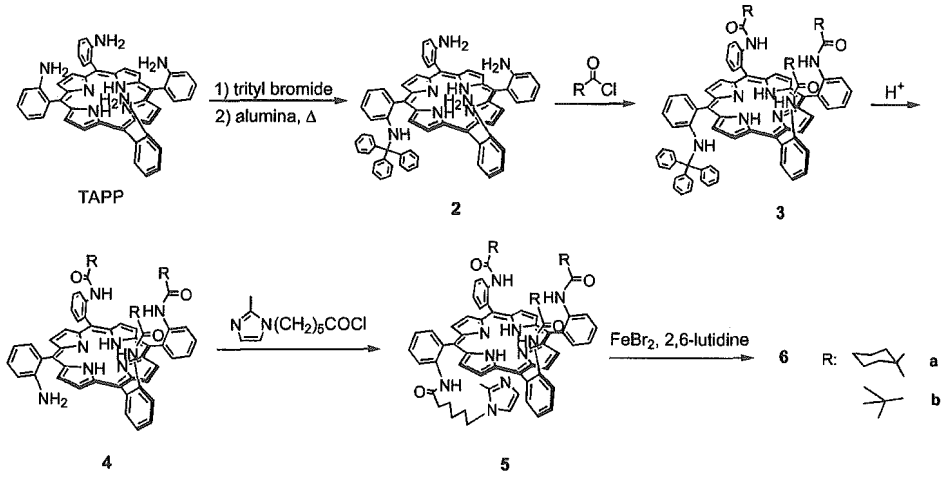

(50%), and (ii) there is no need to modify the porphyrin ring because the proximal base is attached to the fourth β-*o*-NH_2 group of the phenyl ring. This convenient synthetic procedure is a great advantage for the industrial scale-up of the manufacturing of the albumin–heme solution. However, we were not certain of the stability of the O_2-adduct complex of the tailed porphyrinatoiron(II) in an aqueous medium. It has been postulated that the four substituents were essential for preventing an unfavorable proton-driven oxidation of the central ferrous ion of the Fe^{2+}TPP derivatives in water (*1a*, *3*).

First, we describe the synthesis and stereochemistry of the 2-methylimidazole-tailed porphyrinatoirons (**6a**, **6b**) and compare their O_2-binding properties in toluene solution. The effects of the substituents on the O_2-binding parameters are discussed. Furthermore, the O_2-binding property of the albumin–heme hybrid including the tailed porphyrinatiron(II) **6a** has been characterized under physiological conditions. The 5 wt % albumin–heme solution involving the easily prepared **6a** could be the most promising artificial O_2 carrier suitable for mass production.

EXPERIMENTAL SECTION

Synthesis of Tailed Porphyrinatoirons. Experimental details of the synthesis and spectra (^{1}H NMR, IR, UV–Vis, HR-MS) are supplied as Supporting Information.

Reduction of Ferric Complex to Ferrous Complex in Toluene. Reduction to the porphyrinatoiron(II) was carried out using toluene-aq $Na_2S_2O_4$ in a heterogeneous two-phase system under an N_2 atmosphere as previously reported (*9*). After separation of the two phases, the organic layer containing the ferrous complex was transferred to a 1-cm quartz cuvette under an N_2 atmosphere. The UV–Vis absorption spectra were recorded by a JASCO V-570 spectrophotometer.

Preparation of Albumin–Heme Hybrid. The HSA (Albrec, 25 wt %) was obtained from the NIPRO Corp. (Osaka). Aqueous ascorbic acid (15 mM, 20 μL) was added to an ethanol solution of the porphyrinatoiron(III) derivative (37.5 μM, 4 mL) under CO. After complete reduction of the central ferric ion, the UV–Vis absorption spectrum showed the formation of the six-coordinated carbonyl complex. This ethanol solution was slowly injected into the phosphate buffered solution (pH 7.3, 8 mL) of HSA (9.38 μM) through a Teflon tube under a pressure of CO stream. The mixture was dialyzed using a cellulose membrane against phosphate buffer (pH 7.3) for 2 and 15 h at 4 °C. The ethanol concentration should be reduced to less than 100 ppm. Finally, the total volume was adjusted to 15 mL, thus producing the carbonyl albumin–heme solution (heme/HSA = 4 (mol/mol), [Fe]: 20 μM). The water was deionized using an ADVANTEC GS-200 system.

O_2-Coordination Equilibria and Kinetics. The O_2-binding affinity ($P_{1/2}$) of the porphyrinaoitron(II) in organic solvents or their albumin–hemes in aqueous solution were determined by the spectral changes at various partial pressures of O_2 in previous reports (*2*, *10*). The heme concentrations of 20 μM were normally used for the UV–Vis absorption spectroscopy. The spectra were recorded within the range of 350–700 nm. The O_2-association and -dissociation rate constants (k_{on}, k_{off}) were measured by a competitive rebinding technique (*11*, *12*) using a Unisoku TSP-1000WK-WIN time-resolved spectrophotometer with a Spectron Laser system SL803G-10 Q-switched Nd:YAG laser, which generated a 532 nm pulse of 6-ns duration (10 Hz).

Magnetic Circular Dichroism (MCD). The MCD for the phosphate buffered solutions (pH 7.3) of HSA–**6a** (20 μM) under N_2, O_2, and CO atmospheres were measured using a JASCO J-820 circular dichrometer fitted with a 1.5 T electromagnet at 25 °C. The accumulation times were normally five, and each spectra were subtracted by ones without the electromagnetic as a baseline.

RESULTS AND DISCUSSION

Synthesis of Tailed Porphyrinatoiron. The tailed porphyrinatoirons, **6a** and **6b**, can be synthesized via four reaction steps from TAPP with 6-{*N*-(2-methyl-1-imidazolyl}hexanoic acid (Scheme 1), and their structures were determined by IR, UV, mass and NMR (^{1}H NMR, H–H COSY, Nuclear Overhauser effect (NOE) experiment) spectroscopies. First, TAPP was monotritylated using tritylbromide at room temperature. Statistically, six atrop isomers of the monotritylated compound are formed. Collman and co-workers reported the superior synthesis of tris(α,α,α-aminopheny)-mono(β-tritylaminophenyl)porphyrin (**2**) using the alumina absorption technique in the dark (*13*). We isolated two major components from the reaction mixture according to the procedure with the R_f values (chloroform/ethyl acetate = 1:1 (v:v)) of 0.75 (compound **A**) and 0.90 (compound **B**). The coupling reaction of compound **A** with pivaloyl chloride gave a single product, tris(pivalamido)phenyl-monotritylphenyl-porphyrin (compound **A1**). On the other hand, the same coupling reaction of compound **B** provided two products (compounds **B1** and **B2**) with R_f values (chloroform/ethyl acetate = 2:1 (v/v)) of 0.68 and 0.62, respectively. The mass spectra of the above three compounds exactly demonstrated the same value (calcd. for $C_{78}H_{73}N_8O_3$: 1169.5806), indicating that **A1**, **B1**, and **B2** are atrop isomers. In ^{1}H NMR spectra of **A1** and **B1**, the peaks derived from the CH_3 protons in the pivalamide groups were

Scheme 2. Atropisomers of 2 and Their Pivalamide Derivatives

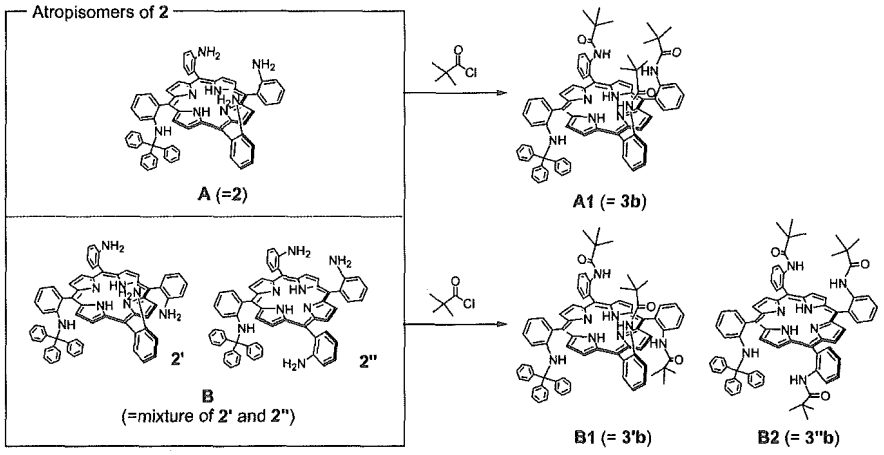

clearly separated into two peaks, and the patterns resembled those of the other $\alpha^3\beta$-structured TAPP derivatives (*14*, *15*) (see Figures ESI1−ESI3, Supporting Information). The differences in the chemical shift between the two peaks were 0.12 (**A1**) and 0.15 (**B1**) ppm, respectively. The CH_3 peaks of **B2** were also splited, but the peak separation was rather small, 0.01 ppm.

To clarify the stereochemistry of these atrop isomers and the geometry of the substituents, we employed the NOE differential spectra (*16*) (see Figures ESI1−ESI3, Supporting Information). In porphyrin **A1**, three pivalamide groups are directed toward the same side and a trityl group is directed only toward the other side, which means **A1** is the target compound **3b**. In **B1**, one of the pivalamide groups is in the same plane with the trityl group, but they do not interact with each other. This result suggests the formation of the $\alpha,\beta,\alpha,\beta$-conformer **3'b**. In **B2**, at least one pivalamide group is on the same side with the trityl group. In this case, there are four atrop isomers expected, but we concluded **B2** would be the $\alpha,\alpha,\beta,\beta$-structure (**3''b**) because the parent compound **B** was less polar than compound **A** in the $\alpha^3\beta$-conformer. In summary (Scheme 2), (i) compound **A** is porphyrin **2** in the $\alpha^3\beta$-conformer, (ii) compound **B** is a mixture of **2'** ($\alpha,\beta,\alpha,\beta$-conformer) and **2''** ($\alpha,\alpha,\beta,\beta$-conformer). Our attempts to perform the same NOE experiment on **3a** unfortunately failed because it was difficult to saturate only the peak of the 1-methyl group at the bottom of cyclohexane ring. The coupling reaction of **2** with 1-methylcyclohexanoyl chloride gave the desired **3a** (yield: 53%).

After detritylation under acidic conditions, 6-(2-methylimidazole-1-yl)hexanoic acid chloride was reacted with the β-*o*-NH_2 group of **4**. Iron insertions of these free base porphyrins were performed with an excess of $FeBr_2$ with 2,6-lutidine as the base. The total yields of **6a** and **6b** were 15 and 10% from the atrop-isomeric mixture of TAPP. All these compounds are now available in gram quantities.

During the synthesis of the tailed porphyrinatoiron, we are always careful to prevent the atrop isomerizations of the products. The bulky pivalamide or 1-methylcyclohexanamide substituted phenyl rings did not rotate with respect to the porphyrin plane by the ambient light and heating even at 100 °C in toluene for 2 h (*8*). However, the same heating of the detritylated porphyrin **4** afforded two components, the unchanged original **4** and the new one with a lower R_f value. They both showed identical molecular weights. The newly appearing compound is suspected to be the porphyrin **4'** in the α^4-conformer. Tritylation of **4'** again by the same procedure for TAPP with tritylbromide did not proceed at all due to the steric hindrance of the fence groups next to the NH_2 group.

Table 1. Absorption Maxima (λ_{max}) of Tailed Porphyrinatoiron(II) in Toluene

	λ_{max}		
	under N_2	under O_2	under CO
6a	438, 535, 558	426, 550	424, 535
6b	435, 535, 555	422, 546	421, 534
1a	441, 539, 558	424, 552	425, 534
1b[a]	439, 535, 561	422, 550	422, 534

[a] Reference 10b.

Table 2. O_2-Binding Parameters of Tailed Porphyrinatoiron(II) in Toluene at 25°C

	k_{on} (M^{-1} s^{-1})	k_{off} (s^{-1})	$P_{1/2}$ (Torr)
6a	5.8×10^7	5.1×10^4	67
6b	8.6×10^7	5.6×10^4	50
1a[a]	1.8×10^8	4.7×10^4	20
1b[a]	1.6×10^8	7.9×10^4	38

[a] Reference 2.

O_2-Binding Properties of Tailed Porphyrinatoiron(II) in Toluene Solution. UV−Vis absorption spectra of ferrous **6a** and **6b** in toluene solution under an N_2 atmosphere were very similar to those of the five-N-coordinate complexes of **1a** and **1b** (Table 1). This indicates that **6a** and **6b** are also five-N-coordinate high-spin Fe^{2+} complex with an intramolecularly coordinated imidazole tail. Upon bubbling of O_2 gas into these solutions, the absorption spectra immediately changed to that of the well-characterized O_2 adduct complex of the Fe^{2+}TPP derivative. After passing the CO gas, the spectral pattern was converted to the typical carbonyl complex. There is no significant difference in the λ_{max} values of **6a**, **6b**, **1a**, and **1b** within 6 nm.

The binding affinities ($P_{1/2}$), association and dissociation rate constants (k_{on}, k_{off}) of O_2 to the tailed porphyrinatoiron(II)s, **6a** and **6b**, were determined (Table 2). We thought that the reduction of the fence numbers on the porphyrin ring plane from four to three unfastens the steric hindrance around the O_2-coordination site and enhanced the association rate constant of O_2. It is generally recognized that the k_{on} value increases with the relaxing distal steric encumbrance (*1*, *11*, *12*, *15*). However, the reverse was the case. In contrast to our assumption, the k_{on} values of the tailed porphyrinatoirons, **6a** and **6b**, were 3.1- and 1.9-fold lower than the corresponding α^4-conformers (**1a** and **1b**), respectively, while their k_{off} values were nearly the same. This result suggests that the steric hindrances for the O_2 association to **6a** and **6b** are greater than those of **1a** and **1b**. Most probably, three fences on the amide bonds in the $\alpha^3\beta$-

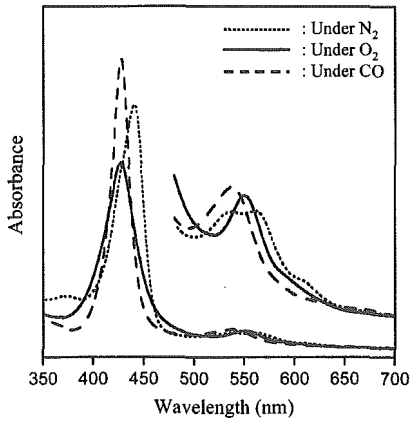

Figure 2. UV−Vis absorption spectral change of HSA−**6a** hybrid in phosphate buffered solution (pH 7.3).

Table 3. Absorption Maxima (λ_{max}) of HSA−Tailed Porphinatoiron (II) Hybrid in Phosphate Buffered Solution (pH 7.3)

	λ_{max}		
	under N_2	under O_2	under CO
HSA-**6a**	440, 536, 559	427, 550	427, 539
HSA-**6b**	–	–	424, 537
HSA-**1a**[a]	445, 543, 567	428, 555	429, 545
HSA-**1b**[a]	443, 542, 567	426, 552	427, 539

[a] Reference 2.

conformer can easily move on the porphyrin platform compared to the crowded four fences of the α^4-conformer. These flexible geometries of the substituents, if anything, narrowed the encumbrance around the O_2-coordination site relative to the α^4 arrangement.

O_2-Binding Properties of HSA-Tailed Porphyrinatoiron in Aqueous Medium. The tailed porphyrinatoirons, **6a** and **6b**, in the $\alpha^3\beta$-conformer could be incorporated into hydrophobic domains of HSA, providing the corresponding albumin−heme hybrids. Their maximum binding numbers to HSA were determined to be approximately 8 (mol/mol), which is identical to those of **1a** and **1b** (*2*, *10a*). It is known that HSA binds porphyrin derivatives and their binding sites largely depend on the chemical structures, hydrophobicity, and electrostaticity. Crystal structure analysis of HSA complexed with natural Fe^{3+} protoporphyrin IX, namely, hemin, revealed that hemin is accommodated into subdomain IB of HSA (*17*). On the other hand, hematoporphyrin is incorporated into subdomain IIIA (*18*), and tetrakis(*p*-sulfonatophenyl)porphyrin binds to subdomain IIA or IIIA (*19*). On the basis of the competitive binding inhibition, we supposed that the some of the binding sites of **1a** are subdomains IB, IIA, and IIIB (*10a*). Attempts to crystallize HSA−**6a** hybrid are now underway, but the porphyrin **6a** dissociated from albumin during the crystallization process due to the relatively low binding constants of **6a** to HSA (10^6−10^4 M^{-1}) and coexistence of poly(ethylene glycol) in the media. We suspect that the binding sites of **6a** and **6b** are the same places of **1a**. The isoelectric point (*p*I = 4.8) and circular dichroism spectral patterns of HSA−**6a** and HSA−**6b** were similar to those of HSA itself, indicating that the surface and conformation of albumin were unaltered after bindings of the tailed porphyrinatoirons.

UV−Vis absorption spectra of the freshly prepared ferrous HSA−**6a** showed λ_{max} values at 424 and 537 nm (Figure 2, Table 3). This spectrum was almost identical to that of the CO coordinated low-spin **6a** in toluene solution, implying that the incorporated tailed porphyrinatoiron(II) is still the CO adduct complex in HSA. Light irradiation to this aqueous HSA−**6a** using a 500-W halogen lamp under an O_2 atmosphere leads to

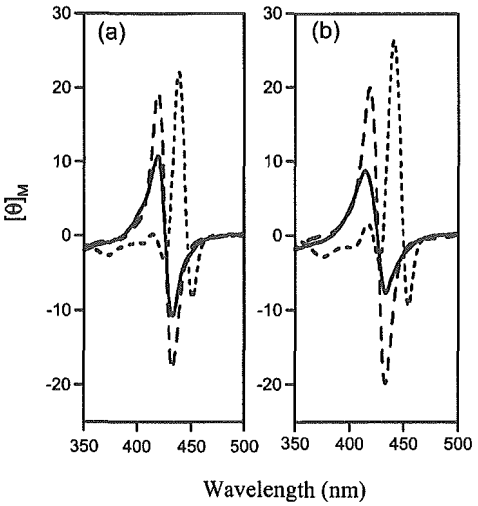

Figure 3. MCD spectral changes of (a) HSA−**6a** and (b) HSA−**1a** hybrids in phosphate buffered solution (pH 7.3). Solid line: under O_2; dotted line: under N_2; dashed line: under CO.

Table 4. O_2-Binding Parameters of HSA−Tailed Porphinatoiron (II) Hybrid in Phosphate Buffered Solution (pH 7.3) at 25°C

	k_{on} (M^{-1} s^{-1})		k_{off} (s^{-1})		
	fast	slow	fast	slow	$P_{1/2}$ (Torr)[a]
HSA−**6a**	2.9×10^7	4.4×10^6	1.1×10^3	1.6×10^2	22 (45)[b]
HSA−**1a**[c]	4.6×10^7	7.3×10^6	9.8×10^2	1.6×10^2	13 (35)[b]

[a] $P_{1/2} = (k_{on}/k_{off})^{-1}$. [b] At 37 °C in parentheses. [c] Reference 2.

CO dissociation, giving a typical spectral pattern of the O_2 adduct complex. Upon exposure of the dioxygenated HSA−**6a** to N_2, the absorption spectrum changed to that of the five-N-coordinated ferrous complex with an intramolecularly coordinated axial imidazole. This O_2 binding and releasing were found to be reversible.

In contrast, the ferrous HSA−**6b** was irreversibly oxidized during the CO dissociation process under an O_2 atmosphere. We concluded that the bulky and hydrophobic substituent like the 1-methylcyclohexanamide fences are necessary for the tailed porphyrinatoiron(II) in the $\alpha^3\beta$-conformer to form a stable O_2 adduct complex under physiological conditions (pH 7.3, 37 °C).

The magnetic circular dichloisim (MCD) spectra of HSA−**6a** showed almost the same pattern as those of HSA−**1b** (Figure 3) (*20*). Under an N_2 atmosphere, the MCD spectrum of HSA−**6a** showed the formation of the five-coordinate ferrous high-spin complex of **6a** with the intramolecular coordinated proximal imidazole. This result showed no ligation of the amino acid residues of the protein, e.g., histidine, tyrosine, cysteine, to the sixth coordination site of the heme. The bulky fences on the porphyrin plane could prevent access of the neighboring peptide residues to the sixth coordination site of **6a**. Upon exposure of this solution to O_2, the spectrum immediately changed and showed an S-shaped A-term MCD in the Soret region, which indicates a transformation to the ferrous low-spin complex (*8*, *21*). The CO adduct complex of HSA−**6a** also exhibited a similar A-term MCD band in the same region with a much stronger intensity. The wavelength where the value of $[\theta]_M$ is zero for the O_2 and CO adduct complex coincided well with the absorption maxima in their corresponding UV−Vis spectra.

The $P_{1/2}$ of the HSA−**6a** was determined by measuring the UV−Vis absorption spectral changes during the O_2 titration. The laser flash photolysis experiments provided the k_{on} and k_{off} values of the O_2 binding to HSA−**6a** (Table 4). The absorption decays accompanying the O_2 recombination were composed of two-phases of the first-order kinetics. The curve was fitted by

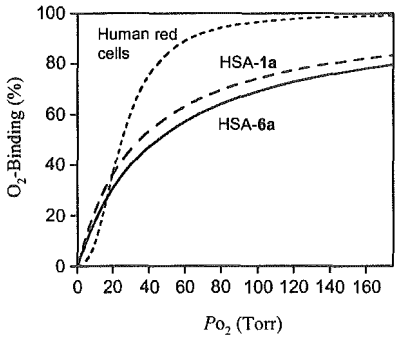

Figure 4. O_2-binding equilibrium curve of HSA−**6a** under physiological conditions (pH 7.3, 37 °C).

a double exponential equation, which was assigned to the fast and slow rebindings [k_{on}(fast) and k_{on}(slow)] of O_2. The k_{on}(fast) values were 7 times greater than k_{on}(slow), and the concentration ratio of the fast and slow reactions was 2:1. This is presumably because the O_2 association to **6a** in HSA is influenced by the molecular microenvironment in the hydrophobic domains (steric hindrance of the amino acid residue and difference in polarity). This behavior was similarly observed in HSA−**1a** and HSA−**1b** (*2*, *22*). The k_{on} values of HSA−**6a** are again 1.6−1.7-fold lower than those of HSA−**1a** in aqueous medium as observed in toluene solution. This is also caused by the narrow encumbrance on the porphyrin ring plane constructed by the three 1-methlcyclohexanamide fences of **6a**.

The HSA−**6a** did not show a cooperative O_2-binding profile like Hb; the Hill coefficient was 1.0 (Figure 4). Although the O_2-binding affinity of HSA−**6a** at 37 °C is relatively low ($P_{1/2}$ value (45 Torr) is high) compared to those of HSA−**1a** (35 Torr) and human red blood cells (28 Torr), the O_2-transporting efficiency of HSA−**6a** between the lungs (Po_2: 110 Torr) and muscle tissues (Po_2: 40 Torr) is estimated to be 22%, which is identical to human red blood cells and HSA−**1a**.

CONCLUSIONS

Tailed porphyrinatoirons have been first employed as an O_2-binding site of the synthetic hemoprotein, albumin−heme. **6a** and **6b** with a β-*o*-(2-methylimidazolyl)hexyramide tail have been easily synthesized via four steps from the TAPP scaffold compared to the eight steps of **1a**. The stereochemistry of the $\alpha^3\beta$-conformer was confirmed by NOE experiments. The association rates of O_2 were slower than for the corresponding α^4-conformers, which indicates that three substituents are close to the porphyrin platform and narrowed the encumbrance space around the O_2-coordination site. As an active site for the albumin−heme hybrid, **6a** was effective, but **6b** was rapidly oxidized. It can be concluded that bulky and hydrophobic substituents like the 1-methylcyclohexanamide fences are necessary for obtaining a stable O_2 adduct complex. The O_2 transporting ability of the HSA−**6a** was almost the same as human red blood cells. Currently, since HSA is manufactured on a large scale by yeast expression (*23*), the 5 wt % albumin−heme solution involving **6a** as O_2 binding site is the most promising material as a red blood cell substitute and O_2-carrying therapeutic reagent, which would be mass produced on an industrial scale.

ACKNOWLEDGMENT

This work was partially supported by Grant-in-Aid for Scientific Research (No. 16350093) from JSPS, Grantin-Aid for Exploratory Research (No. 16655049) from MEXT Japan, and Health Science Research Grants (Regulatory Science) from MHLW Japan.

Supporting Information Available: Synthetic procedure of the tailed porphyrinatoirons (**6a**, **6b**); ^{1}H NMR and NOE differential spectra of compounds **A1**, **B1**, and **B2**. These materials are available free of charge via the Internet at http://pubs.acs.org.

LITERATURE CITED

(1) (a) Collman, J. P., Boulatov, R., Sunderland, C. J., and Fu, L. (2004) Functional analogues of cytochrome *c* oxidase, myoglobin, and hemoglobin. *Chem. Rev. 104*, 561−588. (b) Momenteau, M., and Reed, C. A. (1994) Synthetic heme-dioxygen complexes. *Chem. Rev. 94*, 659−698 and references therein.

(2) Komatsu, T., Matsukawa, Y., and Tsuchida E. (2002) Effect of heme structure on O_2-binding properties of human serum albumin-heme hybrids: Intramolecular histidine coordination provides a stable O_2-adduct complex. *Bioconjugate Chem. 13*, 397−402.

(3) Komatsu, T., Moritake, M., Nakagawa, A., and Tsuchida, E. (2002) Self-organized lipid-porphyrin bilayer membranes in vesicular form: Nanostructure, photophysical properties and dioxygen coordination. *Chem. Eur. J. 8*, 5469−5480.

(4) Komatsu, T., Oguro, Y., Teramura, Y., Takeoka, S., Okai, J., Anraku, M., Otagiri, M., and Tsuchida, E. (2004) Physicochemical characterization of cross-linked human serum albumin dimer and its synthetic heme hybrid as an oxygen carrier. *Biochim. Biophys. Acta 1675*, 21−31.

(5) (a) Huang, Y., Komatsu, T., Yamamoto, H., Horinouchi, H., Kobayashi, K., and Tsuchida, E. (2004) Safety evaluation of an artificial O_2 carrier as a red blood cell substitute by blood biochemical tests and histopathology observations, *ASAIO J. 50*, 525−529. (b) Komatsu, T., Huang, Y., Yamamoto, H., Horinouchi, H., Kobayashi, K., and Tsuchida, E. (2004) Exchange transfusion with synthetic oxygen-carrying plasma protein "albumin-heme" into an acute anemia rat model after seventy-percent hemodilution. *J. Biomed. Mater. Res. 71A*, 644−651. (c) Huang, Y., Komatsu, T., Yamamoto, H., Horinouchi, H., Kobayashi. K., and Tsuchida, E. (2004) Exchange transfusion with entirely synthetic red-cell substitute albumin-heme into rats: physiological responses and blood biochemical tests. *J. Biomed. Mater. Res. 71A*, 63−69.

(6) Kobayashi, K., Komatsu, T., Iwamaru, A., Matsukawa, Y., Horinouchi, H., Watanabe, M., and Tsuchida, E. (2002) Oxygenation of hypoxic region in solid tumor by administration of human serum albumin incorporating synthetic hemes. *J. Biomed. Mater. Res. 64A*, 48−51.

(7) Lindsey, J. (1980) Increased yield of a desired isomer by equilibriums displacement on binding to silica gel, applied to meso-tetrakis(o-aminophenyl)porphyrin. *J. Org. Chem. 45*, 5215−5215.

(8) Collman, J. P., Brauman, J. I., Doxsee, K. M., Halbert, T. R., Bunnenberg, E., Linder, R. E., LaMar, G. N., Gaudio, J. D., Lang, G., and Spartalian, K. (1980) Synthesis and characterization of "tailed picket fence" porphyrins. *J. Am. Chem. Soc. 102*, 4182−4192.

(9) Tsuchida, E., Hasegawa, E., Komatsu, T., Nakata, T., Nakao, K., and Nishide, H. (1991) Synthesis and coordination behaviors of new double-sided porphyrinatoiron(II) complexes: effect of the pocket size for imidazole on dioxygen binding. *Bull. Chem. Soc. Jpn. 64*, 888−894.

(10) (a) Komatsu, T., Hamamatsu, K., Wu, J., and Tsuchida, E. (1999) Physicochemical properties and O_2-coordination structure of human serum albumin incorporating tetrakis-(*o*-pivalamido)phenylporphyrinatoiron(II) derivatives. *Bioconjugate Chem. 10*, 82−86. (b) Tsuchida, E., Komatsu, T., Kumamoto, S., Ando, K., and Nishide, H. (1995) Synthesis and O_2-binding properties of tetraphenylporphyrinatoiron(II) derivatives bearing a proximal imidazole covalently bound at the β-pyrrolic position. *J. Chem. Soc., Perkin Trans. 2*. 747−753.

(11) Collman, J. P., Brauman, J. I., Iverson, B. L., Sessler, J. L., Morris, R. M., and Gibson, Q. H. (1983) O_2 and CO binding to iron(II) porphyrins: A comparison of the "picket fence" and "pocket" porphyrins. *J. Am. Chem. Soc. 105*, 3052−3064.

(12) Traylor, T. G., Tsuchiya, S., Campbell, D., Mitchell, M., Stynes, D., and Koga, N. (1985) Anthracene heme cyclophanes. Steric Effects in CO, O_2 and RNC Binding. *J. Am. Chem. Soc. 107*, 604−614.

(13) Collman, J. P., Broring, M., Fu, L., Rapta, M., Schwenninger, R., and Straumanis, A. (1998) Novel protecting strategy for the synthesis of porphyrins with different distal and proximal superstructures. *J. Org. Chem. 63*, 8082−8083.

(14) Inaba, Y., and Kobuke, Y. (2004) Synthesis of a complementary dimer from mono(imidazolyl)-substituted cobalt(II) porphyrin as a new artificial T-form hemoglobin. *Tetrahedron 60*, 3097−3107.
(15) Wuenschell, G. E., Tetreau, C., Lavalette, D., and Reed, C. A. (1992) Hydrogen-bonded oxyhemoglobin models with substituted picket-fence porphyrins: the model compound equivalent of site-directed mutagenesis. *J. Am. Chem. Soc. 114*, 3346−3355.
(16) Collman, J. P., Sunderland, C. J., and Boulatov, R. (2002) Biomimetic studies of terminal oxidases: trisimidazole picket metalloporphyrins. *Inorg. Chem. 41*, 2282−2291.
(17) Zunszain, P. A., Ghuman, J., Komatsu, T., Tsuchida, E., and Curry, S. (2003) Crystal structural analysis of human serum albumin complexes with hemin and fatty acid, *BMC Struct. Biol. 3*, 6.
(18) Cohen, S., and Margalit, R. (1990) Binding of porphyrin to human serum albumin, structure−activity relationship. *Biochem. J. 270*, 325−330.
(19) Andrade, S. M., and Costa, S. M. B. (2002) Spectroscopic studies on the interaction of a water soluble porphyrin and two drug carrier proteins. *Biophys. J. 82*, 1607−1619.
(20) Tsuchida, E., Nakagawa, A., and Komatsu, T. (2003) Coordination structure of active site in synthetic hemoprotein (albumin-heme) with dioxygen and carbon monoxide. *Macromol. Symp. 195*, 275−280.
(21) (a) Collman, J. P., Brauman, J. I., Collins, T. J., Iverson, B. L., Lang, G., Pettman, R. B., Sessler, J. L., and Walters, M. A. (1983) Synthesis and characterization of the "pocket" porphyrins. *J. Am. Chem. Soc. 105*, 3038−3052. (b) Collman, J. P., Basolo, F., Bunnenberg, E., Collins, T. C., Dawson, J. H., Ellis, P. E., Marrocco, M. L., Moscowitz, A., Sessler, J. L., and Szymanski, T. (1981) Use of magnetic circular dichroism to determine axial ligation for some sterically encumbered iron(II) porphyrin complexes. *J. Am. Chem. Soc. 103*, 5636−5648.
(22) Komatsu, T., Matsukawa, Y., and Tsuchida, E. (2000) Kinetics of CO and O_2 binding to human serum albumin-heme hybrid. *Bioconjugate Chem. 11*, 772−776.
(23) Sumi, A., Ohtani, W., Kobayashi, K., Ohmura, T., Yokoyama, K., Nishida, M., and Suyama, T. (1993) Purification and physicochemical properties of recombinant human serum albumin. *Biotechnology of Blood Proteins* (Rivat, C., Stoltz, J.-F., Eds.) Vol. 227, pp 293−298, John Libbey Eurotext, Montrouge.

BC050154+

Poly(ethylene glycol)-Conjugated Human Serum Albumin Including Iron Porphyrins: Surface Modification Improves the O_2-Transporting Ability

Yubin Huang,[†] Teruyuki Komatsu,[†,*] Rong-Min Wang,[†,‡] Akito Nakagawa,[†] and Eishun Tsuchida[†,*]

Advanced Research Institute for Science and Engineering, Waseda University, 3-4-1 Okubo, Shinjuku-ku, Tokyo 169-8555 Japan, and Key Laboratory of Polymer Materials of Gansu Province, Institute of Polymer, Northwest Normal University, Lanzhou 730070, China. Received November 3, 2005; Revised Manuscript Received February 10, 2006

Artificial O_2-carrying hemoprotein composed of human serum albumin including tetrakis(*o*-amidophenyl)-porphinatoiron(II) (Fe4P or Fe3P) [HSA−FeXP] has been modified by maleimide- or succinimide-terminated poly(ethylene glycol) (PEG), and the formed PEG bioconjugates have been physicochemically characterized. 2-Iminothiolane (IMT) reacted with the amino groups of Lys to create active thiol groups, which bind to α-maleimide-ω-methoxy PEG [Mw: 2-kDa (PEG_{M2}), 5-kDa (PEG_{M5})]. On the other hand, α-succinimidyl-ω-methoxy PEG [Mw: 2-kDa (PEG_{S2}), 5-kDa (PEG_{S5})] directly binds to Lys residues. MALDI-TOF MS of the PEG-conjugated HSA−FeXP showed distinct molecular ion peaks, which provide an accurate number of the PEG chains. In the case of PEG_{MY}(HSA−FeXP), the spectroscopic assay of the thiol groups also provided the mean of the binding numbers of the polymers, and the degree of the modification was controlled by the ratio of [IMT]/[HSA]. The viscosity and colloid osmotic pressures of the 2-kDa PEG conjugates (phosphate-buffered saline solution, [HSA] = 5 g dL^{-1}) were almost the same as that of the nonmodified one, whereas the 5-kDa PEG binding increased the rheological parameters. The presence of flexible polymers on the HSA surface retarded the association reaction of O_2 to FeXP and stabilized the oxygenated complex. Furthermore, PEG_{MY}(HSA−FeXP) exhibited a long circulation lifetime of FeXP in rats (13−16 h). On the basis of these results, it can be concluded that the surface modification of HSA−FeXP by PEG has improved its comprehensive O_2-transporting ability. In particular the PEG_{MY}(HSA−FeXP) solution could be a promising material for entirely synthetic O_2-carrying plasma expander as a red cell substitute.

INTRODUCTION

Poly(ethylene glycol) (PEG) is commonly used for the surface modification of peptides, proteins, enzymes, and liposome to confer several potential beneficial effects: not only a longer plasma half-life and nonimmunogenicity but also a solubility in organic solvents and extreme thermostability (*1*−*4*). To develop an artificial O_2 carrier, substantial efforts have been directed to the preparation of PEG-conjugated hemoglobin (Hb) over the past decades (*5*−*8*), and the optimized PEG−Hbs are currently being tested in clinical trials. Human serum albumin (HSA) is a versatile protein, which is found in our blood plasma at a high concentration (4−5 g dL^{-1}) (*9*). We have reported that HSA including tetrakis(*o*-amidophenyl)porphinatoiron(II) (Fe3P or Fe4P, Chart 1) [HSA−FeXP] can reversibly bind and release O_2 under physiological condition (pH 7.4, 37 °C) in a fashion similar to Hb (*10*). The administration of this synthetic O_2 carrier into anesthetized rats has proved its safety and O_2-transporting efficacy (*11*). Nevertheless, there is only one defect in that the FeXP molecule easily dissociates from HSA when infused into animals. This is due to the fact that FeXP is noncovalently bound to the hydrophobic cavity of albumin with binding constants (K) of 10^4−10^6 (M^{-1}). Natural heme, namely protoporphinatoiron IX, is also incorporated into HSA and shows a 10^2−10^4-fold higher K compared to FeXP (*12*); however, it is released from HSA during blood circulation with a half-life of 2.5−3.6 h (*13*, *14*). Under these circumstances,

Chart 1. Structures of O_2-Adduct Complexes of Tetrakis-(*o*-amidophenyl)porphinatoiron(II)

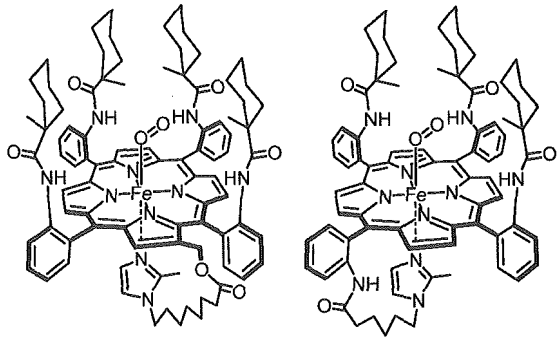

Fe4P Fe3P

we postulated that the surface modification of HSA−FeXP by PEG could help to prolong the circulation life of FeXP and thereby retain its O_2-transporting ability for a long period. Although HSA is a very common plasma protein, its PEG conjugation chemistry has not yet been studied in detail. It is known that a huge variety of drugs are incorporated into specific sites of HSA (*9*). The PEG modification should prevent the rapid release of these drugs from the HSA scaffold and contribute to raising their potential therapeutic efficacies.

In the present study, we have systematically prepared several PEG-conjugated HSA−FeXPs and characterized their physicochemical properties. The surface modification by PEG affects the viscosity and colloid osmotic pressure of the solution, O_2-binding behavior of the parent HSA−FeXP, and circulatory lifetime of FeXP. The PEG-conjugated HSA−FeXP could be

* Corresponding authors: (E.T.) Tel: +81-3-5286-3120, Fax: +81-3-3205-4740, E-mail: eishun@waseda.jp. (T.K.) E-mail: teruyuki@waseda.jp; eishun@waseda.jp.

[†] Waseda University.

[‡] Northwest Normal University.

10.1021/bc050315+ CCC: $33.50
Published on Web 02/22/2006 PAGE EST: 5.8

of extreme medical importance as a red cell substitute or O_2-therapeutic reagent.

EXPERIMENTAL PROCEDURES

Materials and Apparatus. All reagents were purchased from commercial sources as special grades and used without further purification. 2-Iminothiolane hydrochloride (IMT) was purchased from Wako Pure Chemical Industries, Ltd. (Osaka, Japan). α-[3-(3-Maleimido-1-oxopropyl)amino]propyl-ω-methoxy PEG [averaged Mw: 2333 (Sunbright ME-020MA, PEG_{M2}), averaged Mw: 5207 (Sunbright MEMAL-50H, PEG_{M5})] and α-succinimidyloxyglutaryl-ω-methoxy PEG [averaged Mw: 2325 (Sunbright MEGC-20HS, PEG_{S2}), averaged Mw: 5261 (Sunbright MEGC-50HS, PEG_{S5})] were purchased from NOF Corp. (Tokyo, Japan). 2-{8-(2-Methylimidazolyl-1-yl)-octanoyloxymethyl}-5,10,15,20-tetrakis{α,α,α,α-*o*-(1-methylcyclohexanamido)phenyl}porphinatoiron(III) chloride (Fe4P) and 5,10,15-tris{α,α,α-*o*-(1-methylcyclohexanamido)-phenyl}-20-mono-[β-*o*-{6-(2-methylimidazolyl) hexanamido}-phenyl]porphinatoiron(III) chloride (Fe3P) were synthesized using previously reported procedures (*10d,e*). Recombinant HSA was provided by the NIPRO Corp. (Osaka, Japan). The UV−vis absorption spectra were recorded using an Agilent 8453 UV−visible spectrophotometer fitted with an Agilent 89090A temperature control unit. The water was deionized using Millipore Elix and Simpli Lab-UV.

Preparation of PEG-Conjugated HSA−FeXP. The HSA−FeXP solutions (X = 3, 4, [HSA]: 5 g dL^{-1}, [FeXP]/[HSA]= 4 (mol/mol), pH 7.4) were prepared as described elsewhere (*10b,d*).

PEG_{MY}(HSA−FeXP): The modification of HSA−FeXP by α-maleimide-ω-methoxy PEG_{M2} was, for instance, carried out as follows. IMT (72 mg, 0.54 mmol) was slowly added to the HSA−FeXP solution (48 mL, [HSA]: 5 g dL^{-1}, [Fe4P] = 3 mM, pH 7.4) ([IMT]/[HSA] = 15/1, mol/mol) and gently stirred at room temperature in the dark. After 3 h, PEG_{M2} (1.44 g, [PEG_{M2}]/[HSA]:20/1, mol/mol) was added to the mixture, which was continually stirred for another 2 h. The resultant solution was ultrafiltered and washed by at least a 600 mL of phosphate-buffered saline (PBS) solution (pH 7.4) to remove any unreacted IMT and PEG_{M2} using the ADVANTEC UHP-76K holder with a Q0500 076E membrane (cutoff Mw: 50 kDa). The volume was finally condensed to 48 mL and sterilized by a DISMIC 0.45 μm filter, producing the PEG_{M2}(HSA−FeXP) solution. The FeXP concentration was determined by the assay of the iron ion by inductively coupled plasma (ICP) spectrometry using a Seiko Instruments SPS 7000A Spectrometer. The HSA concentration was calculated from the intensity of the circular dichroism spectrum at 208 nm, because the molar ellipticity of HSA (1.9×10^4 deg cm^2 $dmol^{-1}$) was unaltered after the PEG conjugation. Circular dichroism (CD) spectra were obtained using a JASCO J-725 spectropolarimeter. The concentration of the HSA sample was 0.15 μM in PBS, and quartz cuvettes with a 10-mm thickness were used for the measurements over the range of 195−250 nm. The PEG_{M2}(HSA−Fe3P) and PEG_{M5}-(HSA−Fe4P) solutions were also prepared by the same procedure. The product was sealed in a glass bottle under CO pressure and stored at 4 °C.

PEG_{SY}(HSA−Fe4P): The surface modification of HSA−Fe4P by α-succinimidyl-ω-methoxy PEG_{S2} was carried out as follows. PEG_{S2} (0.72 g, 0.36 mmol) was directly added to the HSA−Fe4P solution ([HSA]: 5 g dL^{-1}, [Fe4P] = 3 mM, pH 7.4) ([PEG_{S2}]/[HSA]:10/1, mol/mol), and the mixture was stirred at room temperature for 2 h. The resultant solution was ultrafiltered, condensed (48 mL), and sterilized as described above, producing the PEG_{S2}(HSA−Fe4P) solution. Using PEG_{S5} instead of PEG_{S2}, PEG_{S5}(HSA− Fe4P) was obtained. The Fe4P and HSA concentrations were determined by the same procedures for PEG_{MY}(HSA−FeXP).

Matrix-Associated Laser Desorption Ionization Time-of-Flight Mass Spectra (MALDI-TOF MS). The MALDI-TOF MS were obtained using a Shimadzu/Kratos AXIMA-CFR S/W Version 2, which was calibrated by BSA (Sigma A-0281) and HSA (Sigma A-3782). The specimens were prepared by mixing the aqueous sample solution (10 μM, 1 μL) and matrix (10 mg mL^{-1} sinapinic acid in 40% aqueous CH_3CN, 1 μL) on the measuring plate and air-drying.

Determination of Mean of PEG_{MY} Chains per Protein by Assay of Thiol Groups. The active thiol groups on the protein surface can be assayed by the disulfide exchange reaction with 2,2′-dithiopyridine (2,2′-DTP) to produce 2-thiopyridinone (2-TP) with an absorption at 343 nm (molar absorption coefficient (ϵ_{343}): 8.1×10^3 M^{-1} cm^{-1}) (*15*). Quantitative spectroscopic measurements conveniently provide the thiol concentration. The parent HSA−FeXP showed a small absorption band in this range, which should be subtracted from the spectrum after the disulfide exchange reaction. The difference in the thiol groups per HSA−FeXP before and after the PEG_{MY} modification corresponds to the mean of the PEG_{MY} chains on the protein surface.

Solution Properties. The viscosity and density of the PEG-conjugated HSA−FeXP solution (PBS, pH 7.4) were obtained using an Anton Paar DSC 300 capillary viscometer at 37 °C. The colloid osmotic pressures of the solutions (PBS, pH 7.4) were measured by a WESCOR 4420 Colloid Osmometer at 25 °C. A membrane filter with a 30 kDa cutoff was used.

O_2-Binding Parameters. O_2-binding to PEG-conjugated HSA−FeXP was expressed by eq 1,

$$\text{PEG(HSA−FeXP)} + O_2 \underset{k_{off}}{\overset{k_{on}}{\rightleftharpoons}} \text{PEG(HSA−FeXPO}_2\text{)} \quad (1)$$

where $K = k_{on}/k_{off}$. The O_2-binding affinity (gaseous pressure at half O_2 binding for FeXP, $P_{1/2} = 1/K$) was determined by spectral changes at various partial pressures of O_2/N_2 as previously reported (*10b,d*). The FeXP concentrations of 10−20 μM were normally used for the UV−vis absorption spectroscopy. The spectra were recorded within the range of 350−700 nm. The half-lifetime of the O_2-adduct complex was determined by the time dependence of the absorption intensity at 550 nm (O_2-adduct species). The association and dissociation rate constants for O_2 (k_{on}, k_{off}) were measured by a competitive rebinding technique using a Unisoku TSP-1000WK laser flash photolysis as reported in a previous paper (*16*).

Circulation Lifetime in Vivo. The animal investigations were carried out using twenty male Wistar rats (297 ± 29 g). All animal handling and care were in accordance with the NIH guidelines. The protocol details were approved by the Animal Care and Use Committee of Keio University. The PEG-conjugated HSA−FeXP solution (20% volume of the circulatory blood) was intravenously injected into rats from the tail vein (1 mL/min) under an inhalation anesthesia with diethyl ether (n = 4 each). Blood was taken from the tail vein at 3, 30 min, 1, 2, 4, 8, 16 h, 1, 2, 3 days (10 time points) after the infusion and then centrifuged to isolate the serum, which was colored brown by the presence of the sample. The animals were sacrificed after the experiments by hemorrhage. The FeXP concentration was measured by an iron ion assay using ICP spectrometry as described above.

RESULTS AND DISCUSSION

Synthesis of PEG-Conjugated HSA−FeXP. The HSA−FeXP molecules were conjugated with PEG having a terminal reactive chain-end, maleimide-PEG or succinimide-PEG, at

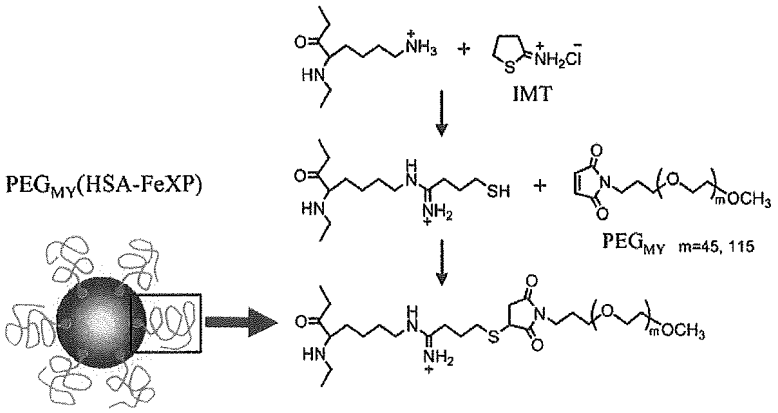

Figure 1. Two-step reaction schemes of IMT and maleimide-PEG (PEG$_{MY}$) with HSA−FeXP.

ambient temperature. Thiolation regent, IMT, quantitatively reacted with the amino groups of Lys to create active thiol groups, which bind to the α-maleimide-ω-methoxy PEG (PEG$_{M2}$ or PEG$_{M5}$) (Figure 1). The two-step reaction is reproducible and did not form any toxic side-product. On the other hand, the α-succinimidyl-ω-methoxy PEG (PEG$_{S2}$ or PEG$_{S5}$) directly binds to the amino groups of Lys. The gel permeation chromatogram (Sephacryl 200HR) of the well-washed PEG conjugate exhibited a single band, so that we did not need any further chromatographic purification.

The MALDI-TOF MS of PEG$_{M5}$(HSA−Fe4P), as prepared under the condition of [IMT]/[HSA−Fe4P] = 15/1 (mol/mol), showed five distinct ion peaks at 85, 90, 95, 101, and 106 kDa (Figure 2a). No unreacted HSA−FeXP was observed at all. The difference in each mass was 5.25 kDa, which implies that HSA−Fe4P is covalently bound to PEG$_{M5}$ and the individual peaks are attributed to PEG$_{M5}$(HSA−Fe4P) having a different number of PEG chains. Here, we have to be cautious whether these mass values involve a molecular weight of Fe4P, because our previous MALDI-TOF MS experiments of HSA−Fe4P demonstrated a single peak of HSA (Mw: 66.5 kDa); the incorporated Fe4P dissociated from the albumin during the ionization process (*10a*). In this study, we found that the mean of the surface PEG chains on HSA−FeXP is conveniently determined by a spectroscopic assay of the HSA scaffold and thiol groups. In general, the concentration of HSA is measured by the absorption at 280 nm or bromcresol green method (*17*), but they are probably obstructed by the surface modification. We then employed a CD measurement to determine the HSA concentration. The comparison of the CD spectra of HSA and PEG−HSA solutions revealed that the molecular ellipcity of albumin (ϵ_{208} = 1.9 × 10^4 deg cm^2 dmol^{-1}) is unaltered even after the PEG binding. Moreover, the presence of FeXP does not disturb the CD in the range of 190−250 nm. Therefore, the HSA concentration of PEG modified HSA−FeXP was quantitatively determined by its CD intensity at 208 nm. On the other hand, the active thiol groups on proteins are generally assayed by a disulfide exchange reaction with 2,2′-DTP (*15*). The combination of these two methodologies allows us to estimate the number of thiols on HSA−FeXP. The mean of the thiol groups was 6.7 per protein after the thiolation by IMT ([IMT]/[HSA−Fe4P] = 15 mol/mol) and decreased to 0.6 after the reaction with 20-fold excess moles of PEG$_{M5}$ (Table 1). These results suggested that the mean of 6.1 reactive thiols was conjugated with PEG$_{M5}$. The averaged molecular weight of this PEG$_{M5}$(HSA−FeXP) calculated from the intensity of the MS peak was 95 kDa. If one subtracts the total mass of the six PEG$_{M5}$ chains (5 kDa × 6 = 30 kDa) from 95 kDa, the difference of 65 kDa equals that

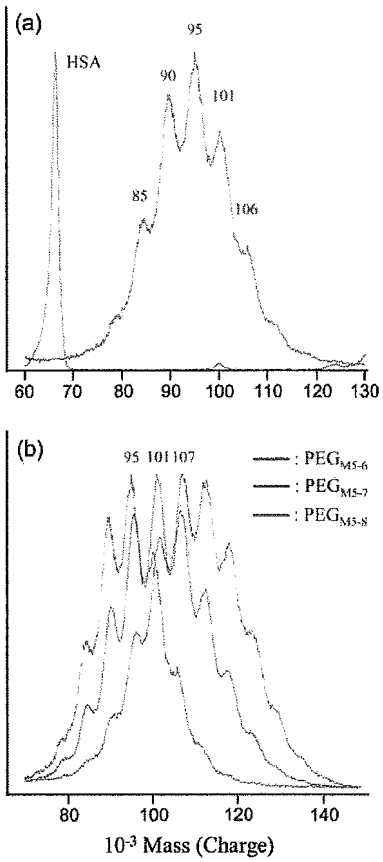

Figure 2. MALDI-TOF MS of (a) HSA and PEG$_{M5-6}$(HSA−Fe4P) and (b) PEG$_{M5}$(HSA−Fe4P) prepared in different [IMT]/[HSA−Fe4P] ratios of 15 (red), 20 (blue), and 30 (green) (mol/mol).

of HSA without Fe4P. Therefore, we concluded that all the mass ion peaks observed in the MALDI-TOF MS did not include the molecular weight of FeXP.

The number of the meleimide-PEG$_{M5}$ chains on HSA−Fe4P were modulated by the mixing ratio of [IMT]/[HSA−Fe4P] (mol/mol). The maximum peak of PEG$_{M5}$(HSA−Fe4P) in the MALDI-TOF MS significantly shifted to the higher molecular region (95 → 101 → 107 kDa) by increasing the IMT (Figure 2b). It is quite remarkable that the distributions of the entire spectral pattern were always identical. The averaged binding number of the PEG$_{M5}$ chains per HSA estimated from the intensity of the mass peak was consistent with the number determined from the assay of the thiol groups (Table 1).

Table 1. The Mean of Thiol Groups per HSA−Fe4P Molecule and Binding Number of the PEG Chains

PEG	[IMT]/[HSA−Fe4P] mol/mol	thiol groups per HSA after IMT addition (A)	thiol groups per HSA after PEG binding (B)	decreased thiol groups (B − A)[a]	averaged PEG number from MS
PEG_{M2}	10	5.6	0.5	5.1	4.6
	15	6.6	0.9	5.7	5.7
	20	8.3	1.1	7.2	6.6
PEG_{M5}	15	6.7	0.6	6.1	5.9
	20	8.0	0.9	7.1	7.2
	30	9.3	1.1	8.2	8.3

[a] This number corresponds to the binding numbers of PEG_{MY} on the protein surface.

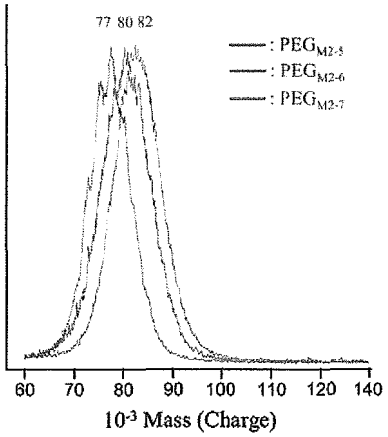

Figure 3. MALDI-TOF MS of PEG_{M2}(HSA−Fe4P) prepared in different [IMT]/[HSA−Fe4P] ratios of 10 (blue), 15 (red), and 20 (green) (mol/mol).

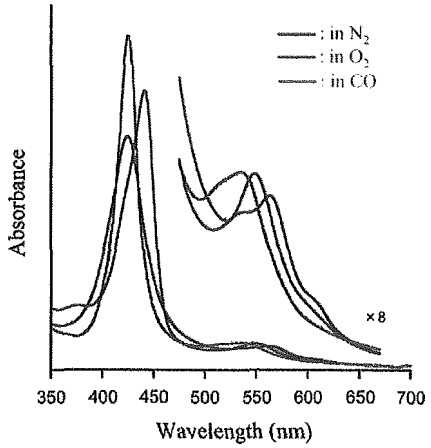

Figure 4. UV-vis absorption spectral change of PEG_{M2-6}(HSA−Fe4P) in PBS solution (pH 7.4).

Table 2. Solution Properties of PEG-Conjugated HSA−FeXP Solutions at 37 °C (pH 7.4, [FeXP] = 3 mM)

PEG	density (g/cm^3)	viscosity (cP)	COP (mmHg)
PEG_{M2-5}(HSA−Fe4P)	1.01	1.08	22
PEG_{M2-6}(HSA−Fe4P)	1.01	1.14	27
PEG_{M2-7}(HSA−Fe4P)	1.01	1.17	28
PEG_{M2-6}(HSA−Fe3P)	1.01	1.14	26
PEG_{M5-6}(HSA−Fe4P)	1.01	2.34	65
PEG_{S2-6}(HSA−Fe4P)	1.01	1.14	22
PEG_{S5-6}(HSA−Fe4P)	1.01	2.30	45
HSA−Fe4P	1.01	1.05	21
HSA	1.01	1.00	21

On the contrary, PEG_{M2}(HSA−Fe4P) demonstrated only one broad peak, because the difference in each mass is relatively close compared to the PEG_{M5} conjugate. The peak maxima of PEG_{M2}(HSA−Fe4P) also shifted to the higher region, dependent on the [IMT]/[HSA−Fe4P] ratio (Figure 3, Table 1).

The succinimide-PEG modified HSA−Fe4P showed the same MALDI-TOF MS patterns as PEG_{MY}(HSA−Fe4P) (data not shown). The number of 5-kDa PEG_{S5} chains per protein increased from 4 → 5 → 6 by elevating the ratio of [PEG_{S5}]/[HSA−Fe4P] (mol/mol): 10 → 20 → 30, respectively. However, the introduced 2-kDa PEG_{S2} number was always 6 in the range of [PEG_{S2}]/[HSA−Fe4P] 10−20. The stoichiometry of the PEG_{S2} binding could not be controlled. This is probably due to the hydrolysis of the succinimidyl end group in aqueous media. The concentration assays of [HSA] by CD and [FeXP] by ICP measurements showed that the initial FeXP/HSA ratio, 4/1 (mol/mol), were constant after the PEG conjugation.

Solution Properties. The viscosity and colloid osmotic pressure (COP) of the 2-kDa PEG-conjugates, PEG_{M2}(HSA−FeXP) and PEG_{S2}(HSA−Fe4P) (PBS solution, [HSA] = 5 g dL^{-1}, pH 7.4), were almost the same as those of the nonmodified HSA−FeXP independent of the number of the PEG chains (Table 2). In contrast, the 5-kDa PEG-conjugate solutions, PEG_{M5}(HSA−FeXP) and PEG_{S5}(HSA−Fe4P), showed a high viscosity (2.30−2.34, at a shear rate of 230 s^{-1}) and hyperoncotic property (45−65 mmHg) in comparison to those of HSA−Fe4P and HSA. From the viewpoint of the design of a blood alternative, it has to achieve a COP similar to that of human blood. However, to increase the effectiveness as a plasma expander, the COP should be higher than the physiological level (*18*). Similar approaches have been utilized for hypertonic saline−dextran formulations.

On the other hand, maintenance of the viscosity has recently been proposed as an important mechanism to preserve shear forces in the microcirculation which prevents loss of the functional capillary density (*19*). The latest PEG-Hb product has been designed to approach that of human whole blood (*7*). Anyway, the COP and viscosity of our PEG-conjugated HSA−FeXP can be adjustable to some extent based on the length of the PEG chains (2-kDa, 5-kDa) on the molecular surface.

O_2-Binding Properties. The UV−vis absorption spectrum of the PEG_{M2}(HSA−Fe4P) solution under an N_2 atmosphere showed λ_{max} at 441, 537, 563 nm (Figure 4), which indicates the formation of the ferrous five-N-coordinate high-spin complex of Fe4P with an intramolecular coordinated 2-methylimidazolyl-group (*10b,c, 20*). The other amino acid residue of HSA did not bind to the sixth-coordinate position of the central ferrous ion. Upon flowing O_2 gas through this solution, the spectral pattern shifted to that of the well-defined O_2-adduct complex of the tetrakis(phenyl)porphinatoiron(II) derivatives (λ_{max}: 424, 550 nm) (*10b,c, 20*). This oxygenation was reversibly observed, dependent on the O_2-partial pressure. After exposure of this solution to CO, PEG_{M2}(HSA−Fe4P) produced a very stable CO-adduct complex (λ_{max}: 425, 535 nm). The all maleimide- and succinimide-PEG-conjugated HSA−FeXP solutions showed similar UV−vis absorption spectra under N_2, O_2, and CO atmospheres. These spectral changes were completely the same as that observed in the nonmodified HSA−Fe4P.

Table 3. O_2-Binding Parameters of PEG-Conjugated HSA−FeXP Solution at 25 °C (pH 7.4)

system	k_{on} ($\mu M^{-1} s^{-1}$) fast	k_{on} ($\mu M^{-1} s^{-1}$) slow	k_{off} (ms^{-1}) fast	k_{off} (ms^{-1}) slow	$P_{1/2}$ (Torr)	$\tau_{1/2}$ (h) at 37 °C
PEG_{M2-5}(HSA−Fe4P)	11	5.8	0.16	0.08	38 (11)	13
PEG_{M2-6}(HSA−Fe4P)	12	4.6	0.17	0.07	32 (11)	12
PEG_{M2-7}(HSA−Fe4P)	9.3	4.7	0.16	0.08	35 (13)	12
PEG_{M2-6}(HSA−Fe3P)	15	4.2	0.52	0.14	41 (26)	8
PEG_{M5-6}(HSA−Fe4P)	12	6.2	0.17	0.09	31 (11)	16
PEG_{S2-6}(HSA−Fe4P)	10	4.3	0.14	0.06	36 (11)	13
PEG_{S5-6}(HSA−Fe4P)	12	5.5	0.25	0.11	32 (16)	18
HSA−Fe4P	31	7.3	0.53	0.13	34 (13)	9
HSA−Fe3P	29	4.4	1.1	0.16	45 (22)	4

The time course of the absorption decay after laser flash photolysis determined the association rate constants of the O_2binding to the PEG-conjugated HSA−FeXP (k_{on}). We have previously reported that the O_2-binding reaction to HSA−FeXP was significantly affected by the microenvironment around FeXP in the protein (e.g., steric hindrance of the amino acid residue and difference in polarity) (*10c−e*). As a result, the binding process of O_2 was observed as the sum of the two single-exponentials, giving fast and slow association rate constants [k_{on}(fast) and k_{on}(slow)]. This unique property of HSA−FeXP has been unaltered after the surface modification by PEG, and all kinetics accompanying the O_2 recombinations consisted of two phases (Table 3). Interestingly, their k_{on}(fast) values were 1.9−3.3-fold lower than those of the corresponding HSA−FeXP, independent of the molecular weight (2-kDa or 5-kDa) and the linkage structure of the PEG. The differences observed in the slow phase were smaller. It may be considered that the presence of flexible polymers on the protein surface retarded the diffusion of the O_2 molecule.

The O_2-binding affinities ($P_{1/2} = K(O_2)^{-1}$) of the PEG-modified HSA−FeXP series were determined by measuring the UV−vis absorption spectral changes by O_2/N_2 titration (Table 3). All the PEG conjugates showed almost the same $P_{1/2}$ values relative to that of the original HSA−FeXP, indicating that the O_2-binding equilibria were not influenced by the presence of PEGs. In contrast, the surface modification by PEG delayed the proton-driven oxidation of the $FeXPO_2$ species and prolonged the half-lifetime of the O_2-adduct complex [$\tau_{1/2}(O_2)$]. The PEG_{M5-6}(HSA−Fe4P)O_2 complex showed the longest $\tau_{1/2}(O_2)$ of 16 h at 37 °C, which is greater than those of HSA−Fe4P and natural hemoprotein, myoglobin ($\tau_{1/2}(O_2)$: 12 h at pH 7, 35 °C) (*21*). Basic polymer PEG conjugation might change the local proton concentration of the HSA interior compared to the outer aqueous solution. Actually, it was shown that the surface PEG modification of hemoproteins has modulated the redox behavior of the active heme site (*1*, *2*, *22*).

Circulation Lifetime in Bloodstream of Rats. The circulation persistence of FeXP in the bloodstream after the administration of PEG_{MY-6}(HSA−FeXP) or PEG_{SY-6}(HSA−Fe4P) solution in rats is shown in Figure 5. The concentration decays of the PEG_{MY}(HSA−FeXP) series showed single exponentials, and the half-lifetimes ($\tau_{1/2}$) were 12.9−15.8 h, independent of the molecular weight of the polymers and FeXP structures. These values are much longer than those of the corresponding nonmodified HSA−FeXP (0.6−3.2 h) (*23*). The surface modification by PEG significantly prevented the rapid clearance of the incorporated FeXP and contributed to increasing the O_2-transporting efficacy.

On the contrary, the PEG_{SY}(HSA−Fe4P) series showed biphasic kinetics and a $\tau_{1/2}$ value of 1.5−2.1 h. We have postulated two reasons for this short circulation lifetime. The first reason is the charges of the Lys residues. The maleimide-PEG connects to Lys through the ring-opened IMT, which maintains the positive charge of Lys; therefore, PEG_{MY}(HSA−FeXP) could preserve the total electrostatic potential of albumin. In contrast, the succinimide-PEG directly binds to the amino group of Lys to form the amide bond, thereby reducing the positive charge and alters the surface electrostatic potential. This changing of the molecular charge may influence the rapid clearance of the incorporated FeXP.

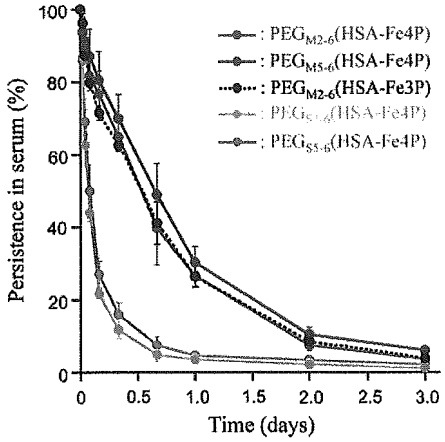

Figure 5. Persistence of FeXP in serum after administration of PEG-conjugated HSA−FeXP into Wistar rats. All values are mean ± SD (n = 4).

The second probability is the binding sites of the PEG chains. As shown in Table 1, the difference in the thiol number per protein before and after the reaction with maleimide-PEG was 0.5−1.1. This means that the binding position of PEG_{MY} is governed by the reaction place of IMT, which is small enough to statistically attach 59 Lys in HSA. Thus, the molecular surface of HSA−FeXP is uniformly covered by PEG_{MY}. On the other hand, the attaching sites of succinimide-PEG are presumably heterogeneous, because PEG_{SY} could only bind the accessible amino group of Lys due to the bulkiness of the long polymer. The incorporated Fe4P molecules might be more easily released from the PEG_{SY}-modified HSA in the circulatory system.

CONCLUSIONS

The surface modification of the albumin-based synthetic hemoprotein, HSA−FeXP, by PEG (Mw 2-kDa or 5-kDa) has improved its comprehensive O_2-transporting ability. The PEG conjugation decreased the O_2-association rate constant but retarded the irreversible oxidation of the central ferrous ion, thereby increasing the stability of the O_2-adduct complex. The 5-kDa PEG conjugation increased the viscosity and COP; however, the 2-kDa PEG conjugation did not change these rheological parameters. The linkage form of the PEG chain dramatically affects the circulation persistence of FeXP. In particular, the maleimide-PEG_{MY} conjugates showed a 6−8-fold longer lifetime compared to the succinimide-PEG_{SY} analogues. This is not dependent on the molecular weight of the polymer chains. In summary, the PEG_{MY}(HSA−FeXP) solution is the most promising candidate as an entirely synthetic O_2-carrying plasma expander for a red cell substitute.

Furthermore, we have recently found that water evaporation of the PEG_{MY}(HSA−FeXP) solution produced a red-colored thin film. Its UV−vis absorption spectrum reversibly changed from the deoxy state under an N_2 atmosphere to the oxy state by exposure to O_2 gas. This PEG_{MY}(HSA−FeXP) film was redissolved in nonaqeuous organic solvents, ethanol, chloroform, etc., and the reversible O_2 binding was again observed. The detailed study of the oxygenations of PEG_{MY}(HSA−FeXP) in a cast film and organic solvent are now underway.

ACKNOWLEDGMENT

This work was partially supported by a Grant-in-Aid for Scientific Research (No. 16350093) from JSPS, a Grant-in-Aid for Exploratory Research (No. 16655049) from MEXT Japan, and Health Science Research Grants (Regulatory Science) from MHLW Japan. Prof. Koichi Kobayashi, Dr. Hirohisa Horinouchi (Keio University), and Mr. Hisashi Yamamoto (NIPRO Corp.) are greatly appreciated for their cooperation with the animal experiments.

LITERATURE CITED

(1) (a) Harris, J. M., Ed. (1992) *Poly(ethylene glycol) Chemistry: Biotechnical and Biomedical Applications*, Plenum Press, New York; (b) Veronese, F. M., Harris, J. M. (2002) Introduction and overview of peptide and protein PEGylation. *Adv. Drug Delivery Rev. 54*, 453−456. (c) Roberts, M. J., Bentley, M. D., Harris, J. M. (2002) Chemistry for peptide and protein PEGylation. *Adv. Drug Delivery Rev. 54*, 459−476.

(2) Veronese, F. M. (2001) Peptide and protein PEGylation: a review of problems and solutions. *Biomaterials 22*, 405−417.

(3) Nucci, M. L., Shorr, R., and Abuchowski, A. (1991) The therapeutic value of poly(ethylene glycol) modified proteins. *Adv. Drug Delivery Rev. 6*, 133−151.

(4) Kawahara, N. Y., and Ohno, H. (1997) Induced thermostability of poly(ethylene oxide)-modified hemoglobin in glycols. *Bioconjugate Chem. 8*, 643−648.

(5) Yabuki, A., Yamaji, K., Ohki, H., and Iwashita, Y. (1990) Characterization of a pyridoxalated hemoglobin-polyoxyethylene conjugate as a physiologic oxygen carrier. *Transfusion 30*, 516−520.

(6) Talarico, T. L., Guise, K. J., and Stacey, C. J. (2000) Chemical characterization of pyridoxalated hemoglobin polyoxyethylene conjugate. *Biochim. Biophys. Acta 1476*, 53−65.

(7) Vandegriff, K. M., Malavalli, A., Wooldbridge, J., Lohman, J., and Winslow, R. M. (2003) MP4, a new nonvasoactive PEG-Hb conjugate. *Transfusion 43*, 509−516.

(8) Manjula, B. M., Tsai, A., Upadhya, R., Perumalsamy, K., Smith, P. K., Malavalli, A., Vandegriff, K., Winslow, R. M., Intaglietta, M., Prabhakaran, M., Friedman, J. M., and Acharya, A. S. (2003) Site-specific PEGylation of hemoglobin at Cys-93(β): correlation between the colligative properties of the PEGylated protein and the length of the conjugated PEG chain. *Bioconjugate Chem. 14*, 464−472.

(9) Peters, T. (1996) *All about Albumin: Biochemistry, Genetics and Medical Applications*, Academic Press, San Diego.

(10) (a) Komatsu, T., Hamamatsu, K., Wu, J., and Tsuchida, E. (1999) Physicochemical properties and O_2-coordination structure of human serum albumin incorporating tetrakis-(*o*-pivalamido)phenylporphyrinatoiron(II) derivatives. *Bioconjugate Chem. 10*, 82−86. (b) Tsuchida, E., Komatsu, T., Matsukawa, Y., Hamamastu, K., and Wu, J. (1999) Human serum albumin incorporating tetrakis(*o*-pivalamido)phenylporphinatoiron(II) derivative as a totally synthetic O_2-carrying hemoprotein. *Bioconjugate Chem. 10*, 797−802. (c) Komatsu, T., Matsukawa, Y., and Tsuchida, E. (2000) Kinetics of CO and O_2 binding to human serum albumin-heme hybrid. *Bioconjugate Chem. 11*, 772−776. (d) Komatsu, T., Matsukawa, and Y., Tsuchida E. (2002) Effect of heme structure on O_2-binding properties of human serum albumin-heme hybrids: Intramolecular histidine coordination provides a stable O_2-adduct complex. *Bioconjugate Chem. 13*, 397−402. (e) Nakagawa, A., Komatsu, T., Iizuka, M., and Tsuchida, E. (2006) Human serum albumin hybrid incorporating tailed porphyrinatoiron(II) in $\alpha,\alpha,\alpha,\beta$-conformer as an O_2 binding site. *Bioconjugate Chem. 17*, 146−151.

(11) (a) Komatsu, T., Huang, Y., Yamamoto, H., Horinouchi, H., Kobayashi. K., and Tsuchida, E. (2004) Exchange transfusion with synthetic oxygen-carrying plasma protein "albumin-heme" into an acute anemia rat model after seventy-percent hemodilution. *J. Biomed. Mater. Res. 71A*, 644−651. (b) Huang, Y., Komatsu, T., Yamamoto, H., Horinouchi, H., Kobayashi. K., and Tsuchida, E. (2004) Exchange transfusion with entirely synthetic red-cell substitute albumin-heme into rats: physiological responses and blood biochemical tests. *J. Biomed. Mater. Res. 71A*, 63−69.

(12) Adams, P. A., and Berman, M. C. (1980) Kinetics and mechanism of the interaction between human serum albumin and monomeric hemin. *Biochem. J. 191*, 95−102.

(13) Russo, S. M., Pepe, J. A., Donohue, S., Cable, E. E., Lambrecht, R. W., and Bonkovsky, H. L. (1995) Tissue distribution of zinc-mesoporphyrin in rats: relationship to inhibition of heme oxygenase. *J. Pharmacol. Exp. Ther. 272*, 766−774.

(14) Komatsu, T., Huang, Y., and Tsuchida, E. (2005) paper in preparation.

(15) Pedersen, A. O., and Jacobsen, J. (1980) Reactivity of the thiol group in human and bovine albumin at pH 3−9, as measured by exchange with 2,2′-dithiodipyridine. *Eur. J. Biochem. 106*, 291−295.

(16) Komatsu, T., Ohmichi, N., Nakagawa, A., Zunszain, P. A., Curry, S., and Tschida, E. (2005) O_2 and CO binding properties of artificial hemoproteins formed by complexing iron protoporphyrin IX with human serum albumin mutants. *J. Am. Chem. Soc. 127*, 15933−15942.

(17) Doumas, B. T., Watson, W. A., and Biggs, H. G. (1971) Albumin standards and measurement of serum albumin with bromcresol green. *Clin. Chim. Acta 31*, 87−96.

(18) Vandegriff, K. D., McCarthy, M., Rohlfs, R., and Winslow, R. M. (1997) Colloid osmotic properties of modified hemoglobins: chemically cross-linked versus polyethylene glycol surface-conjugated. *Biophys. J. 69*, 23−30.

(19) Tsai, A. G., Friesenecker, B., and McCarthy, M. (1998) Plasma viscosity regulates capillary perfusion during extreme hemodilution in hamster skinfold model. *Am. J. Physiol. 275*, H2170−80.

(20) Tsuchida, E., Komatsu, T., Kumamoto, S., Ando, K., and Nishide, H. (1995) Synthesis and O_2−Binding properties of tetraphenylporphyrinatoiron(II) derivatives bearing a proximal imidazole covalently bound at the β-pyrrolic position. *J. Chem. Soc., Perkin Trans. 2* 747−753.

(21) Sugawara, Y., Shikama, K. (1980) Autoxidation of native oxymyoglobin. *Eur. J. Biochem. 110*, 241−246.

(22) Ohno, H. and Tsukuda, T (1992) Electron-transfer reaction of polyethylene oxide-modified myoglobin in polyethylene oxide oligomera. *J. Electroanal. Chem. 341*, 137−149.

(23) Tsuchida, E., T. Komatsu, T., Hamamatsu, K., Matsukawa, Y., Tajima, A.; Yoshizu, A., Izumi, Y., and Kobayashi, K. (2000) Exchange transfusion of albumin-heme as an artificial O_2-infusion into anesthetized rats: physiological responses, O_2-delivery and reduction of the oxidized hemin sites by red blood cells. *Bioconjugate Chem. 11*, 46−50.

BC050315+

Artificial Cells, Blood Substitutes, and Biotechnology, 34: 1–10, 2006

ISSN: 1073-1199 print/1532-4184 online
DOI: 10.1080/00207450500428204

Taylor & Francis
Taylor & Francis Group

Interaction of Hemoglobin Vesicles, a Cellular-Type Artificial Oxygen Carrier, with Human Plasma: Effects on Coagulation, Kallikrein-Kinin, and Complement Systems

Hideki Abe, Mitsuhiro Fujihara, Hiroshi Azuma, and Hisami Ikeda
Hokkaido Red Cross Blood Center, Sapporo, Japan

Kenji Ikebuchi
Department of Transfusion Medicine, Saitama Medical School Hospital, Saitama, Japan

Shinji Takeoka and Eishun Tsuchida
Department of Polymer Chemistry, Advanced Research Institute for Science and Engineering, Waseda University, Tokyo, Japan

Hideyoshi Harashima
Laboratory for Molecular Design of Pharmaceutics and COE Program in the 21st Century, Graduate School of Pharmaceutical Sciences, Hokkaido University, Sapporo, Japan

Abstract: Hemoglobin vesicles (HbVs), cellular-type artificial oxygen carriers containing human hemoglobin, were assessed for their biocompatibility by mixing with human plasma *in vitro*. Among three kinds of HbVs (PEG-DPEA-HbV, PEG-DPPG-HbV and DPPG-HbV), PEG-DPEA-HbV did not affect the extrinsic or intrinsic coagulation activities of the plasma, while PEG-DPPG-HbV and DPPG-HbV tended to shorten the intrinsic coagulation time. The kallikrein-kinin cascade of the plasma was slightly activated by PEG-DPPG-HbV

This study was supported, in part, by a Health Science Research Grant (Artificial Blood Project) from the Ministry of Health and Welfare, Japan, and by Grants-in-Aid for Scientific Research from the Japanese Ministry of Education, Science, Sports and Culture.

Address correspondence to Hideki Abe, Ph.D., Hokkaido Red Cross Blood Center, Japanese Red Cross, Yamanote 2-2, Nishi-ku, Sapporo 063-0002, Japan. E-mail: abeh@hokkaido.bc.jrc.or.jp

and DPPG-HbV, but not by PEG-DPEA-HbV. The complement consumption of the plasma was observed by incubation with DPPG-HbV, but not with PEG-DPEA-HbV or PEG-DPPG-HbV. These results indicate that PEG-DPEA-HbV has a higher biocompatibility with human plasma.

Keywords: Oxygen carrier; Liposome; Hemoglobin vesicles; Complement; Kallikrein-Kinin

INTRODUCTION

Hemoglobin vesicles (HbVs) are human hemoglobin encapsulated into a lipid bilayer (*i.e.* liposome) with a polyethylene glycol (PEG) surface modification and have been developed as an artificial oxygen carrier. We have been evaluating the biocompatibility of the HbVs *in vitro* using human blood. So far, we have revealed that HbVs hardly activated platelets in terms of the aggregation response, p-selectine expression and the release of RANTES [1,2]. For neutrophils, HbVs have the least effect on the chemotactic activity, gelatinase B release, up-regulation of Mac-1 expression and superoxide production triggered by f-MLP [3]. On the basis of these experiments, HbVs appeared to have an acceptable biocompatibility to human blood.

In general, liposomes interact with various kinds of biological components *in vitro* and *in vivo*. The interaction depends on the liposome characteristics such as particle size, surface charge, lipid composition and surface modification. It is widely recognized that negatively charged liposomes activate complement in the rat, guinea pigs and humans [4–6], resulting in rapid removal from the blood circulation as opsonized liposomes by the reticuloendothelial system. A negatively charged surface triggers the intrinsic coagulation pathway and kallikrein-kinin cascade by activating coagulation factor XII (FXII) [7,8]. In addition, the cholesterol contents affects the complement activation [5,9], which is thought to be mediated by natural antibodies [10].

Incorporation of the PEG-conjugate lipid into liposomes (PEGylation) has been reported to be efficacious to avoid these biological responses [11–13]. Indeed, liposome-encapsulated hemoglobin (LEH), which was not PEGylated, has induced complement activation *via* both the classical and alternative pathways in human serum containing natural anti-phospholipid antibodies [14]. These phenomena become of great concern as a pseudoallergic reaction [15,16], which was already observed in a pig model [17]. Recently, however, it has been reported that not only LEH but also PEGylated-liposomes induce hypotension, flushing, respiratory distress, decrease of mean arterola pressure and chest pain [18,19].

In this study, we have used three modified HbVs and assessed their effects on plasma coagulation activity, the kallikrein-kinin cascade and the complement system using human blood. The results obtained here have reinforced the higher biocompatibility of HbVs.

MATERIALS AND METHODS

Liposomes

HbVs were prepared as previously described [20,21]. Briefly, hemoglobin solution prepared from outdated red blood cells for transfusion was heated under a CO gas atmosphere to inactivate possibly contaminated viruses and to remove the stroma and non-hemoglobin proteins [22]. After the removal of impurities by centrifugation and filtration, hemoglobin solution was encapsulated into liposomes by mixing with lipids. The liposomes were then extruded through membrane filters with a pore size of 0.22 μm. Three kinds of HbVs were prepared in this study and the lipid composition (mol%) was as follows: dipalmitoyl phosphatidylcholine (DPPC):cholesterol (CHOL):dipalmitoyl phosphatidylglycerol (DPPG):polyethylene glycol-conjugated distearoyl phosphatidylethanolamine (PEG5000-DSPE) = 5:5:1:0.033 (designated PEG-DPPG-HbVs); DPPC:CHOL:DPPG = 5:5:1 (DPPG-HbVs); DPPC:CHOL:dipalmitoyl-L-glutamate-*N*-succinic acid (DPEA):PEG5000-DSPE = 5:5:1:0.033 (PEG-DPEA-HbVs). All lipids were purchased from Nippon Fine Chemical Co. (Osaka, Japan) except PEG5000-DSPE, which was from NOF Co. (Tokyo, Japan). HbVs were suspended in saline and each of them contains 10 g of Hb/dL, 5.7 g lipids/dL and <0.1 endotoxin unit of lipopolysaccharide/mL. Empty liposome (Coatsome EL-A, 3.1 g lipids/dL) was purchased from NOF Co. and the lipid composition (mol%) was DPPC:CHOL:DPPG = 30:40:30. The particle size and surface charge as the zeta potential of HbVs suspended in saline were measured by Photal ELS-8000HO (OTSUKA Electronics, Tokyo, Japan).

Measurement of Coagulation Activity

Human plasma was prepared from voluntary donated whole blood at Japanese Red Cross blood centers and was stored at $-80^{\circ}C$ until use. The prothrombin time (PT) and activated partial thromboplastin time (APTT) as an extrinsic and intrinsic coagulation system, respectively, were determined using a physical clotting assay on a coagulation analyzer

(KC10; Amelung, Lehbrinksweg, Germany) at several mixing ratios with plasma and liposomes. Reagents for these assays were purchased from Dade International Inc. (Miami, FL). PT and APTT were measured according to the manufacturer's instructions. Briefly, the mixtures at ratios of 20:80, 40:60 or 60:40 (v/v) of plasma:HbVs or saline were dispensed into a sample cup in duplicate. After the addition of reagents, time to coagulation was measured automatically.

Detection of Kallikrein Activation

The presence of kallikrein activation was evaluated as the degradation of high-molecular-weight kininogen (HMWK), which is substrate of kallikrein naturally existing in the plasma. HMWK was purchased from Enzyme Research Laboratories Inc. (South Bend, IN); anti-human HMWK light chain antiserum from Nordic Immunological Laboratories (Capistrano Beach, CA); plasma kallikrein from Sigma Chemical Co. (St Louis, MO). Plasma was incubated with HbVs or saline at ratios of 80:20, 60:40 or 40:60 (v/v) at 37°C for 24 h. After centrifugation at 15,000 g for 45 min at 4°C, supernatants were treated with 1% sodium dodecyl sulfate (SDS) and 1% 2-mercaptoethanol at 95°C for 10 min and then electrophoresed on a 5–20% gradient polyacrylamide gel containing 0.1% SDS. After proteins were transferred from the gel to nylon membrane, the membrane was treated primarily with anti-HMWK serum, and secondly with anti-goat IgG antibody labeled with horseradish peroxidase. HMWK was detected with a chemiluminescence detection system (ECL; Amersham, Buckinghamshire, UK). Single chain HMWK (S-HMWK) (33 μg) was digested with plasma kallikrein (6 mU) at 37°C for 2 h. Both digested and undigested S-HMWK were used as standards for Western blot analysis.

Measurement of Complement Titer

Human serum was prepared from whole blood of voluntary donors and stored at −80°C until use. Serum was incubated with HbVs, EL-A or saline at ratio of 80:20 or 60:40 (v/v) at 37°C for 1 h. After centrifugation at 15,000 g for 45 min at 4°C, supernatants were stored at −80°C until assay. The complement titer was measured using a 50% hemolysis assay based on Mayer's method with a commercial kit (New One point CH50 (KW); Japan BCG Supply Co., Tokyo, Japan). Therefore, the units of the complement titer were expressed as CH50.